A data-model synthesis to explain variability in calcification observed during a CO_2 perturbation mesocosm experiment

Shubham Krishna[1] and Markus Schartau[1]

[1]GEOMAR Helmholtz Centre for Ocean Research Kiel, Düsternbrooker Weg 20, 24105 Kiel, Germany

Correspondence to: Shubham Krishna (skrishna@geomar.de) and Markus Schartau (mschartau@geomar.de)

Abstract. The effect of ocean acidification on growth and calcification of the marine algae *Emiliania huxleyi*, was investigated in a series of mesocosm experiments where enclosed water volumes that comprised a natural plankton community were exposed to different carbon dioxide (CO_2) concentrations. Calcification rates observed during those experiments were found to be highly variable, even among replicate mesocosms that were subject to similar CO_2 perturbations. Here, data from an ocean acidification mesocosm experiment are reanalysed with an optimality-based dynamical plankton model. According to our model approach, cellular calcite formation is sensitive to variations in CO_2 at the organism-level. We investigate the temporal changes and variability in observations, with focus on resolving observed differences in total alkalinity and particulate inorganic carbon (PIC). We explore how much of the variability in the data can be explained by variations of the initial conditions and by the level of CO_2 perturbation. Nine mesocosms of one experiment were sorted into three groups of high, medium and low calcification rates and analysed separately. The spread of the three optimised ensemble model solutions captures most of the observed variability. Our results show that small variations in initial abundance of coccolithophores and the prevailing physiological acclimation states generate differences in calcification that are larger than those induced by ocean acidification. Accordingly, large deviations between optimal mass flux estimates of carbon and of nitrogen are identified even between mesocosms that were subject to similar ocean acidification conditions. With our model-based data analysis we document how an ocean acidification response signal in calcification can be disentangled from the observed variability in PIC.

1 Introduction

Much knowledge about growth and mortality of phytoplankton has been inferred from experiments where environmental factors like light, temperature, and nutrient availability have been predominantly controlled, e.g. in laboratory experiments with batch cultures or with chemostats. Typically, these experiments are designed to determine a physiological response to variations of a single factor, e.g. explaining changes in photosynthetic rate when exposed to different light conditions (e.g. Platt et al., 1977; Marra and Heinemann, 1982; Lewislg and Smith, 1983; Geider et al., 1985; Harrison and Platt, 1986; Harding Jr et al., 1987). Many laboratory experiments are performed with monocultures, with the advantage that physiological responses may then become well expressed in measurements while variability between replicates or even between repeated experiments should remain low. In this context a series of laboratory studies with monocultures of calcifying coccolithophores were conducted to investigate responses in calcification to variations in carbonate chemistry, often with *Emiliania huxleyi*, (e.g.

Zondervan et al., 2002; Iglesias-Rodriguez et al., 2008; Langer et al., 2009; Barcelos e Ramos et al., 2010). These studies were motivated by the expectation that the observed trend in OA will affect calcifying algae and that their physiology is likely sensitive to the seawater's calcite saturation state (Feely et al., 2004; Orr et al., 2005).

The repeated laboratory OA experiments showed ambiguous responses in calcification to variations in carbon dioxide (CO_2) concentrations and Findlay et al. (2011) pointed out that differences in laboratory methodology, but also details in experimental design, are likely the reason for the large observed variability in *E. huxleyi* responses to changes in carbonate chemistry. Similarly, Engel et al. (2014) stressed that variations in the observed ratio between particulate inorganic carbon and particulate organic carbon (PIC:POC ratio) increase with the decrease of measured relative growth rates, depending on whether "low" growth conditions were balanced (as achieved with chemostats) or resulted from unresolved transient nutrient-limitation effects in batch cultures. This ongoing discussion is accompanied by the question of how representative the outcomes of monoculture laboratory experiments are, to allow for reliable future projections of OA effects on oceanic calcification rates of coccolithophores and on possible climate feedbacks.

If we seek to make inference about future changes in calcification under oceanic conditions, experimental data are needed that consider more realistic environmental conditions with a natural phytoplankton community that may include calcifying algae like *Emiliania huxleyi*. A series of studies were conducted to investigate effects of OA on plankton dynamics. Among those were experiments with tanks or bags called mesocosms, with some enclosed water volume that typically comprised a natural plankton community. These mesocosms were typically perturbed and exposed to different CO_2 concentrations, e.g. Pelagic Ecosystem CO_2 Enrichment (PeECE) studies (Riebesell et al., 2008). Few studies focused on the impact of OA on growth of *E. huxleyi*. In contrast to monoculture laboratory experiments, CO_2 perturbation mesocosm experiments yield "net" community response signals that are anticipated to be more indicative for possible future changes in oceanic calcification of coccolithophores. Replicate mesocosms with similar initial nutrient, as well as initial dissolved inorganic carbon (DIC) concentrations typically show comparable temporal response patterns, i.e. an exponential growth phase until nutrients become depleted and a post-bloom period where chlorophyll *a* concentrations decline. However, replicate mesocosms that all included *E. huxleyi* exhibited large deviations in calcification responses, thereby altering carbonate chemistry. Such variability was well reflected in total alkalinity (TA) measurements of the PeECE-I experiment (Delille et al., 2005). Furthermore, during PeECE-I it happened that mesocosms with high and low calcification rates were revealed among replicates in all three CO_2 treatments. To find enhanced variability in calcification in mesocosm experiments is comprehensable and can be attributed to the likely mixture of superimposed responses of multiple plankton species even within replicates of similar CO_2 perturbation. Thus, small deviations in the initial relative mass distribution of photoautotrophs, zooplankton, and detritus between replicate mesocosms can translate into some pronounced variability in measurements even under similar environmental conditions (e.g. Eggers et al., 2014).

Here we investigate data and their variability of replicate mesocosms during the PeECE-I experiment. For this we take a modelling approach to simulate environmental conditions and the predominant dynamics of nine individual mesoscosms as described in Engel et al. (2005) and in Delille et al. (2005). Joassin et al. (2011) presented a dynamical model to simulate the mass flux of carbon (C), nitrogen (N), and of phosphorus (P) for the same PeECE-I experiment. Their model resolves growth

and losses of *E. huxleyi* together with interdependencies between bacteria, viruses, detritus, and dissolved organic matter (DOM). The model of Joassin et al. (2011) also features the exudation and coagulation process of dissolved polysaccharides (here referred to as dissolved combined carbohydrates, dCCHO) to form transparent exopolymer particles (TEP). In the study of Joassin et al. (2011) some emphasis is put on the enhanced mortality of *E. huxleyi* due to viral lysis and on the variable stoichiometry (C:N ratio) of the particulate organic matter (POC:PON ratio). They did not attempt to resolve a dependency between calcification and CO_2 concentration and therefore restricted their simulations to one treatment with three replicate mesocosms that were exposed to present day CO_2 concentrations.

The focus of our model approach is different in that we distinguish between two phytoplankton functional types, calcifying algae (e.g. *E. Huxleyi*) and bulk non-calcifying algae, i.e. an unresolved combination of picoplankton, dinoflagellates and diatoms. We assume a CO_2 sensitivity for the ratio of calcification to net carbon fixation (photosynthesis minus respiration), based on results from the meta-analysis of Findlay et al. (2011). In our data-model synthesis we concentrate on the initialisation (initial filling) of the mesocosms, with possible variations in the relative distribution of plankton and detritus resolved in our model. A data assimilation (DA) method is employed for the estimation of parameter values, which helps to disentangle and understand some of the differences and commonalities seen in observations, in particular in TA and PIC data, but also in measurements of dissolved inorganic nitrogen (DIN) and DIC, chlorophyll *a*, as well as in particulate organic nitrogen (PON) and POC.

First we will briefly provide some background information about the experimental setup of PeECE-I, including irradiance, temperature and salinity, as these environmental factors enter our model simulations. This will be followed by a description of the model equations that include components of the optimality-based approach to simulate algal growth, using parameterisations proposed by Pahlow et al. (2013). Thereafter, the data assimilation method for parameter estimation will be briefly explained. Specific details of the model and of the data assimilation method are given in the Appendix. Ensembles of three distinct model solutions will be presented together with their mass flux estimates of C and N. We will discuss the problem of identifying initial conditions in combination with important model parameters. We will also address the problem of resolving the variability observed in the accumulation of PIC and how this variability is related to the expression of the CO_2 effect introduced to the model.

2   Material and methods

For our analysis we consider the setup and data of the PeECE-I experiment, a study conducted at the Marine Biological Field Station (Raunefjorden, 60.3°N, 5.2°E) of the University of Bergen, Norway between 31 May and 25 June 2001 (Engel et al., 2005; Delille et al., 2005). The objective of this study was to investigate OA effects on marine calcifying algae (coccolithophores) captured in polyethylene bags of enclosed water volumes (mesocosms) and perturbed by different levels of CO_2 concentrations. A dynamical plankton ecosystem model is used for simulations of N and carbon C flux within each mesososm. We apply a data assimilation method to identify best estimates of model parameter values together with initial conditions for model simulations.

2.1 Experimental data

Nine mesocosms of 2 m diameter and 11 m^3 volume were filled with unfiltered, post-bloom, nutrient depleted water from the fjord. After the filling of the mesocosms, nutrients were added so that all mesocosms had similar initial nutrient concentrations, approximately 15 mmol m^{-3} of nitrate together with nitrite and 0.5 mmol m^{-3} of phosphate. Like the nutrients, the initial total

5 alkalinity (TA) in all nine bags were 2146 mmol m^{-3} approximately (or if normalised to unit mass ≈ 2200 μmol kg^{-1}). The bags were covered with air-tight tents of tetra-fluroethylene foil that allowed 95% of photosynthetically active radiation (PAR) to pass through. The mesocosm bags were subject to three different levels of perturbation of partial pressure of CO$_2$: a) mesocosms 1-3, referred to as M1, M2, and M3, were exposed to similarly high DIC levels (initial DIC = 2119 mmol m^{-3} , 2119 mmol m^{-3} , 2122 mmol m^{-3}) with 700 ppmV of initial pCO$_2$, b) M4, M5, and M6 started from DIC = 2048 mmol

10 m^{-3} , 2056 mmol m^{-3} , 2040 mmol m^{-3} with a corresponding pCO$_2$=370 ppmV, and treatment c) with initial DIC = 1919 mmol m^{-3}, 1929 m^{-3}, 1927 m^{-3} with 180 ppmV pCO$_2$ in mesocosms M7, M8, and M9. Thus, data from three replicate mesocosms are available for each of the three CO$_2$ treatments. For each mesocosm the partial pressure of atmospheric CO$_2$ above the surfaces was largely controlled by a continuous injection of gas with a treatment specific, individually prescribed CO$_2$ content. Because there was an open space between surface of mesocosms and the tents, we assumed the pCO$_2$ in the

15 air above the mesocosms' surfaces to be a mixture of 90% of the pertubed pCO$_2$ inside a mesocosm and 10% of the actual atmospheric pCO$_2$ (340 ppm) in all replicates.

Daily samples were collected and measured over a period of 23 days. For every mesocosm temperature and salinity data were interpolated to hourly values for direct use as environmental input for model simulations (Fig. 1). Hourly photosynthetic available radiation (PAR) data were derived from meteorological global irradiance measurements of the Geophysical institute

20 at Bergen (Skartveit et al., 2001). Figure (1) shows that temperature increased by approximately 3 Degree Celsius during the experiment and variations between the different mesocosms remained small. Small but noticeable differences exist between mesocosms with respect to salinity. In all mesocosms a gradual decrease in salinity was observed, from S=31.3 to approximately S=30.8. The PAR data exhibit variations on an hourly scale, due to changes in cloud cover.

2.2 Modelling approach

25 For model simulations we assume that all mesocosms are homogeneously mixed, as we neglect an explicit representation of vertical turbulent mixing (0D-model approach). Furthermore, we assume no light gradient in mesocosms and use depth integrated hourly irradiance data to force the model. The applied model equations describe mass exchange rates of N and C between compartments of 1) dissolved inorganic nitrogen and carbon (DIN and DIC), 2) N and C biomass of coccolithophores and other phytoplankton (CoccoN and CoccoC , PhyN and PhyC), 3) zooplankton (ZooN and ZooC), and 4) detritus (DetN

30 and DetC), and 5) labile dissolved organic N and C (DON and DOC), Fig. (2). As due to the design of the PeECE-I experiment our model includes some additional features. . The first is that we consider an explicit representation of dissolved combined carbohydrates (dCCHO) that act as precursors for transparent exopolymer particles (TEPC), similar to Schartau et al. (2007) and Joassin et al. (2011). Since our model resolves changes in TA along with DIC so that we can also derive pH values and the

corresponding partial pressure of CO_2 (pCO_2). We neither resolve viral infections nor bacterial biomass explicitly, as done in Joassin et al. (2011). Microbial activity is implicitly considered by parameterisations of hydrolysis and remineralisation. Both processes are assumed to be temperature dependent but are independent of changes in bacteria biomass. Instead, hydrolysis and remineralisation rates are calculated as being proportional to substrate availability only. Likewise, any effects by viral lysis remain unspecified and are an integral part of a single total mortality that is assigned to phytoplankton and coccolithophores. In the following, the general model equations of mass flux of C and N are described as sources and sinks, inducing changes in the mass concentration of the respective state variables.

2.2.1 Photoautotrophs

In our model we distinguish between calcifying and non-calcifying photoautotrophs, coccolithophores (Cocco) and other bulk phytoplankton (Phy). Respective net photoautotrophic growth rates ($\mu_{\text{cocco/phy}}$) are described as rates of gross carbon fixation (V^C) minus some corresponding sum of respiration costs (r_C) due to the synthesis of chlorphyll a, nutrient assimilation, and maintenance: $\mu_{\text{cocco/phy}} = V^C - r_C$. The proportions of V^C and r_C are determined by optimal resource allocation while energetic trade-offs are imposed, as described in Pahlow et al. (2008). These physiological equations of optimal allocation have been shown to be well applicable for a series of different conditions (e.g. including diazotrophy) and scales (e.g. Smith et al., 2011; Pahlow et al., 2013; Arteaga et al., 2014; Fernández-Castro et al., 2016). Here we neglect diazotrophy as well as the effect of phosphorus availability on nitrogen uptake and thus on algal growth. From the data we could not infer any phosphorus limitation of growth prior to nitrogen depletion and we assume that cellular nitrogen (N) directly limits the net growth rate of photoautrophs ($\mu_{\text{cocco/phy}}$). Nitrogen is generally necessary for synthesising enzymes. According to the model approach of Pahlow and Oschlies (2009), the major metabolic pathways within the algae are regulated by the resources allocated to produce these enzymes. Thus, key processes like photosynthesis, chlorophyll a synthesis and net carbon fixation become affected by internal resource allocation. The model maximises the photoautotrophic growth rates by optimising the allocation of resources to nutrient acquisition sites and to the light harvesting complex (LHC). The auxiliary variables mentioned above are described in Table A.1 in Appendix (A). The detailed equations are given in Appendix (A.2).

Biomass concentrations of photoautotrophs: The biomass build-up (net growth) of photoautotrophs depends on the amount of N and C assimilated by the algae minus losses because of aggregation, grazing by zooplankton and because of exudation or leakage of organic matter. The sources minus sinks (sms) terms of the photoautotrophs' biomass are:

sms of photoautotroph biomass $= $ C and N uptake $-$ exudation/leakage $-$ aggregation $-$ grazing

The corresponding sms (source minus sink) differential equations of C and N biomass for phytoplankton and coccolithophores are given in Appendix(A.2).

Chlorophyll a concentrations: The synthesis of chlorophyll a (Chl) is represented by an optimal trade-off between photosynthesis and respiratory costs in the chloroplast of a cell. The synthesis rate depends on the degree of light saturation (S_I), on the amount of net carbon fixed inside chloroplasts, and on the chlorophyll-to-carbon ratio (θ). Also, the chlorophyll syn-

thesis rate is sensitive to changes in cellular nitrogen-to-carbon (N:C), Q^N. The descriptions of the above introduced auxiliary variables are given in Table A.1. Like for biomass, the parameterisations for chlorophyll a are identical for the calcifying and non-calcifying phytoplankton in our model:

sms of chlorophyll $a\ =\ $ synthesis of chlorophyll $a -$ aggregation $-$ grazing

The respective differential equations for chlorophyll a of non-calcifying phytoplankton (with subscripts phy) and coccolithophores ($cocco$) are listed in Appendix (A.2).

Formation of particulate inorganic carbon (PIC): The process of calcification in our model depends on the amount of energy provided through photosynthesis and is simply expressed by a ratio of PIC formation per carbon fixed (f_{PIC}, Eq. A.21). The differential equation of PIC describes a net accumulation rate (formation minus dissolution) and no explicit distinctions can be made with respect to how PIC becomes eventually distributed between algal biomass, detritus or zooplankton:

sms of particulate inorganic carbon $=\ $ calcification by coccolithophores $-$ dissolution of coccoliths (calcite)

The differential equations for precipitation and dissolution of PIC are given in Appendix (A.4).

2.2.2 Zooplankton

The grazing losses of the photoautotrophs are resolved with an explicit representation of zooplankton biomass. With our grazing approach (Holling type III) no distinctions are made between micro- and mesozooplankton or between different feeding types. Changes in zooplankton biomass are subject to a mortality (M_{zoo}; e.g. losses to higher trophic levels). Other loss terms represent respiratory costs (r_{zoo}) as well as excretion (γ_{zoo}). Zooplankton restore C and N towards a constant N:C ratio (Q^{zoo}_{const}) of 0.19. The restoring time (τ) in our model is equal to one day. It mimics an increase in respiration (r_{zoo}) if N:C ratio falls below Q^{zoo}_{const} and an increase in excretion (γ^N_{zoo}) if N:C is above Q^{zoo}_{const}. Details of auxiliary variables related to the zooplankton compartment of the model are given in Table A.1. The buildup of zooplankton biomass depends on the total prey concentrations (phytoplankton and coccolithophores):

sms of zooplankton biomass $=\ $ grazing on phytoplankton $+$ grazing on coccolithophore

$$- \text{ respiration (or excretion)} - \text{mortality}$$

The differential equation for zooplankton biomass and grazing function are given in Appendix (A.5).

2.2.3 Detritus

Detritus comprises a variety of components with particles of different sizes and sinking rates (Fasham et al., 1990). The detritus resolved by our model simply combines dead plankton biomass and fecal pellets. Sources of detrital C,- and N mass are given in terms of phytoplankton aggregation and mortality of zooplankton. Aggregation is parameterised with quadratic loss terms of the photoautotrophs. These aggregation equations resolve interactions between two types of particles (small cells of photoautotrophs and large aggregates of detritus): a) aggregation of cells of photoautrophs and b) aggregation of small photoautotrophs with larger detritus, see details in the Appendix (A). The two particle-type approach allows a trade-off between accuracy of estimated mass flux and the resolution of particle size (Ruiz et al., 2002). We assume that hydrolysis is temperature dependent and that it is responsible for the degradation of detritus, acting as a source for (labile) $LDON$ and $LDOC$. The equations of detrital C and N can thus be described as:

$$\textbf{sms of detritus} = \text{aggregation of phytoplankton} + \text{aggregation of coccolithophore}$$
$$+ \text{ zooplankton mortality} - \text{hydrolysis}$$

The respective differential equations of detrital C and N mass are given in the Appendix (A.7).

2.2.4 Dissolved inorganic compounds (DIN, DIC) and total alkalinity (TA)

Dissolved inorganic nitrogen (DIN): The DIN pool represents the total concentration of nitrate, nitrite and ammonium. Nitrogen utilisation by phytoplankton and coccolithophores is a sink of DIN, whereas heterotrophic excretion and remineralisation of $LDON$ are the major sources:

$$\textbf{sms of dissolved inorganic nitrogen} = - \text{ N uptake by phytoplankton} - \text{N uptake by coccolithophores}$$
$$+ \text{ excretion by heterotrophs} + \text{remineralisation}$$

The sms differential equation for DIN is given in Appendix (A.8).

Dissolved inorganic carbon (DIC): The DIC pool combines CO_2, bicarbonate and carbonate. The primary sinks of DIC are net carbon fixation to support photoautotrophic growth ($\mu_{cocco/phy}$) and calcification of coccolithophores. We do not differentiate between the utilisation of CO_2 and bicarbonate for algal growth and calcification. Note that net carbon fixation ($\mu_{\text{cocco/phy}}$) in our model becomes slightly negative in the absence of light (dark respiration of the photoautotrophs). Total heterotrophic respiration acts as major DIC source and is expressed by zooplankton respiration and by the remineralisation of dissolved

organic carbon (LDOC + dCCHO):

sms of dissolved inorganic carbon $= -$ net C uptake by phytoplankton $-$ net C uptake by coccolithophores

$-$ calcification $+$ dissolution of PIC $+$ zooplankton respiration

$+$ remineralisation $+$ gas exchange

The corresponding differential equation for DIC is listed in Appendix (A.8).

Total alkalinity (TA): Temporal changes in TA in our model are due to the sinks and sources of DIN and DIP (ΔDIP $= \frac{1}{16} \cdot \Delta$DIN), process of precipitation and dissolution of calcite plates produced by the calcifying algae. We follow the nutrient-H^+ compensation principle described in Wolf-Gladrow et al. (2007). In our model we are resolving the nitrogen flux of zooplankton excretion but we are eventually not resolving any associated net change in TA (total alkalinity). This is because we cannot differentiate between the excretion of ammonium (NH_4^+) and of nitrate (NO_3^-) and nitrite (NO_2^-). The excretion of one mole NH_4^+ would increase TA by one mole, whereas the excretion of one mole NO_3^- or NO_2^- would decrease TA by one mole (Wolf-Gladrow et al., 2007). In other words, we indirectly impose that half of the N excretion by zooplankton is NH_4^+ and the other half is NO_3^- and NO_2^-, which would introduce a net TA change of zero. Measured values of DIN, TA, and DIC on day one of the experiment were taken as initial conditions for respective mesocosms.

sms of total alkalinity $=$ N and P uptake by phytoplankton $+$ N and P uptake by coccolithophores

$-$ calcification by coccolithophores $+$ dissolution of calcite

$-$ remineralisation of dissolved organic N and P

The differential equation for TA is given in the Appendix (A.8).

2.2.5 Dissolved labile organic matter and transparent exoplymer particles

Dissolved organic matter (DOM) is produced by exudation of the photoautotrophs and by hydrolysis of detrital matter. The DOM is subject to remineralisation, being the source of DIN and DIC. The applied model distinguishes between dissolved combined carbohydrates (dCCHO) and a residual fraction of labile dissolved organic carbon and nitrogen (LDOC and LDON). This distinction is made because only dCCHO are simulated to act as precursors for the formation of transparent exopolymer particles (TEP). In our model the DOM's primary source is freshly exuded and leaked organic matter from photoautotrophs. An addtional source of DOM is due to degradation of detrital matter (hydrolysis and microbial exudation) in response to bacterial activity. The fraction of exudates that enter the dCCHO pool may vary between expontential growth phase and during periods of nutrient limited growth, described as two modes of exudation in Schartau et al. (2007). We therefore introduced a parameterisation ($f_{\text{dCCHO}}^{cocco/phy}$, Eq. A.39) that simulates such shift in quality of the exudates, depending on the respective cell

quota of the coccolithophores and of the other phytoplankton ($Q_{cocco/phy}^{N}$). Remineralisation and microbial respiration are respective sinks of LDOC and LDON. Table A.1 lists all associated auxiliary variables. The equations for labile DOC and DON are described as follows (with details given in Appendix, A.9):

sms of labile dissolved organic matter = exudation by photoautotrophs

$$+ \text{hydrolysis/degradation of detritus} + \text{hydrolysis/degradation of gels}$$

$$- \text{remineralisation/respiration of dissolved organic matter}$$

Dissolved combined carbohydrates (dCCHO): By introducing dCCHO we account for an additional sink of DOC other than microbial degradation, which is the physical-chemical transformation of dissolved to particulate matter, here resolved as the coagulation of dCCHO to form TEP carbon (TEPC). This transformation is parameterised as an aggregation process, as proposed in Engel et al. (2004) and effectually applied in Schartau et al. (2007) and in Joassin et al. (2011), (see details in Appendix, A.10):

sms of dissolved combined carbohydrates = exudation $-$ coagulation of dCCHO

$$- \text{aggregation of dCCHO with TEP} - \text{remineralisation of dCCHO}$$

Transparent exopolymer particles (TEP): The carbon content of TEP (TEPC) is explicitly resolved because it can be a significant constituent of POC measurements (Verdugo et al., 2004). This consideration is important for our data-model synthesis, in particular because it affects the stoichiometric C:N ratio of particulate organic matter. The sink terms of dCCHO, described before, are the only sources for TEPC in our model approach. The degradation of TEPC is parameterised similar to the hydrolysis of detritus:

sms of transparent exopolymer particles (TEPC) = coagulation of dCCHO + aggregation of dCCHO with TEP

$$- \text{degradation}$$

The corresponding differential equation for TEPC production is listed in the Appendix (A.10).

2.2.6 Model parameters and initial conditions

Out of 33 model parameters, 26 parameters are fixed and remaining 7 parameters (4 initial condition parameters (f_{cocco}, f_{zoo}, f_{det}. PON_0) and 3 ecological parameters (α_{phy}, α_{cocco}, Q_0) enter the optimisation procedure. The decision on which parameters should become subject to optimisation is based on a series of preceding parameter optimisations and subsequent sensitivity analyses. A major objective is to reduce the number of parameters for optimisation to a meaningful minimum. This facilitates

the identification of those parameter values that are of primary concern. Since we address differences in initial conditions in our study, we consider four parameters that determine these differences and they need to become subject to optimisation. The additionally selected three growth parameters are amongst those to which the model solution is most sensitive. The model solutions are also highly sensitive to variations of the maximum potential nitrogen uptake rate (V_0^N). This parameter is excluded from optimisation, because it is not possible to obtain estimates of (V_0^N) that are independent of estimates of the photosynthetic efficiency. Therefore, a value is assigned to V_0^N that is typical and was used for simulations of other experiments (e.g. Pahlow et al., 2013), ensuring credible estimates of those parameters that are optimised in our study. The mesocosm experiment covers only a short post-bloom period and we found other parameters, like maximum grazing rates and the aggregation parameters, to be weakly constrained by the available data. Their consideration for optimisation would impede the identification of the other more important parameters. Values assigned to those parameters that are excluded from optimisation are adapted from other studies (e.g. Pahlow et al., 2013; Schartau et al., 2007).

Initial condition values for some of the state variables in the model are computed by initial condition parameters, given in fractions. The initial biomass during the start of the experiments, specified by PON_0, is distributed between living and non-living biomass, which is determined by the parameter of the initial detritus fraction (f_{det}). The living biomass is further distributed between photoautotrophs and zooplankton, specified by the initial zooplankton fraction parameter (f_{zoo}). Finally, the remaining relative distribution of photoautotrophic biomass is set by f_{cocco}. For example, a value of $f_{cocco} = 1$ would mean that all photoautotrophic biomass is associated with the presence of coccolithophores exclusively.

$$PON_0 = DetN_0 + ZooN_0 + CoccoN_0 + PhyN_0 \tag{1}$$

with the individual fractions:

$$DetN_0 = f_{det} \cdot PON_0 \tag{2}$$

$$ZooN_0 = f_{zoo} \cdot (PON_0 - DetN_0) \tag{3}$$

$$CoccoN_0 \quad f_{cocco} \cdot (PON_0 - DetN_0 - ZooN_0) \tag{4}$$

$$PhyN_0 = (1 - f_{cocco}) \cdot (PON_0 - DetN_0 - ZooN_0) \tag{5}$$

For initial zooplankton, coccolithophore and phytoplankton biomass we apply a constant C:N ratio of 6.625. We consider a higher C:N ratio (= $2 \cdot 6.625$) only for initial detritus. Since the mesocosms were filled with post-bloom, nutrient depleted water masses, we assume that all dead particulate organic matter has a C:N ratio that is rather typical for such post-bloom conditions. Initial condition of PIC, DIC, and TA are taken from the data for respective mesocosm, whereas we assume same small fixed values (e.g. DON = 0.05 mmol m^{-3}, DOC = 102.5 mmol m^{-3}, dCCHO = 1.0 mmol m^{-3} and TEPC = 3.5 mmol m^{-3}) as initial conditions for all mesocosms.

2.3 Design of data assimilation (DA) approach

A peculiarity of the PeECE-I experiment is that high and low changes in total alkalinity (TA) were found in all three CO$_2$ treatments, in response to differences in calcification (Delille et al., 2005). Because the three distinct patterns in calcification (Fig.

3) are attributable to all three treatments means that a factor other than the CO_2 perturbations induced variations between the individual mesocosms. For all other observations no such clear pattern could be identified. We designed our data assimilation approach according to this finding and therefore investigate three possible situations (model solutions) that differ in their TA response: low, medium and high calcification (referred to as LC, MC, and HC respectively). Thus, for each of these three (LC, MC and HC) situations we find three mesocosms that were subject to three different CO_2 levels (initial 700 ppmV, 370 ppmV, and 180 ppmV). By adapting the same nomenclature as in Engel et al. (2005) and in Delille et al. (2005), we can assign the mesocosms M1, M6, and M8 to those with low calcification rates (highest TA), M2, M5, and M7 to the ones with medium calcification and finally M3, M4, and M9 to mesocosms with high calcification rates (lowest TA).

2.3.1 Definition of cost function (data-model misfit)

In our data assimilation approach we consider data from the three cases (LC, MC, and HC) separately, but we make identical statistical assumptions. The observation vector $(\boldsymbol{y}_i)$ contains daily means of three mesocosms of the following measurements: 1) dissolved inorganic carbon (DIC, mmol m^{-3}), 2) dissolved inorganic nitrogen (DIN) (nitrate + nitrite, mmol m^{-3}), 3) chlorophyll a (Chl a, mg m^{-3}), 4) particulate organic nitrogen (PON, mmol m^{-3}), 5) particular ogranic carbon (POC, mmol m^{-3}), 6) particulate inorganic carbon (PIC, mmol m^{-3}), 7) total alkalinity (TA, mmol m^{-3}). Like the data vector $\boldsymbol{y}_i$, the vector $H_i(\boldsymbol{x})$ represents mean values of three simulated mesocosms for each calcification case (LC, MC, and HC). It combines results of model states: C and N biomass concentrations of the photoautotrophs (PhyN & PhyC and CoccoN & CoccoC), of zooplankton (ZooN & ZooC), of detritus (DetN & DetC), and carbon concentration of transparent exopolymers particles (TEPC). The vector of differences $(\boldsymbol{d}_i)$ between observation $(\boldsymbol{y}_i)$ and model results $H_i(\boldsymbol{x})$ is given as:

$$\boldsymbol{d_i} = \boldsymbol{y}_i - H_i(\boldsymbol{x}) = \underbrace{\begin{pmatrix} \mathrm{DIC}_i \\ (\mathrm{NO_3^-} + \mathrm{NO_2^-})_i \\ \mathrm{Chl}\ a_i \\ \mathrm{PON}_i \\ \mathrm{POC}_i \\ \mathrm{PIC}_i \\ \mathrm{TA}_i \end{pmatrix}}_{\text{data}} - \underbrace{\begin{pmatrix} \mathrm{DIC}_i \\ \mathrm{DIN}_i \\ (\mathrm{Chl}_{phy} + \mathrm{Chl}_{cocco})_i \\ (\mathrm{PhyN} + \mathrm{CoccoN} + \mathrm{ZooN} + \mathrm{DetN})_i \\ (\mathrm{PhyC} + \mathrm{CoccoC} + \mathrm{ZooC} + \mathrm{DetC} + \mathrm{TEPC})_i \\ \mathrm{PIC}_i \\ \mathrm{TA}_i \end{pmatrix}}_{\text{model\ \ results}} \quad (6)$$

For the cases LC, MC, and HC we calculated daily residual standard errors (σ_i) based on the measurements. Unlike other variables, the estimation of the standard errors for DIC is not straightforward because of the different CO_2 levels. For the derivation of the standard errors we considered the differences (offsets) of the mean *initial* DIC concentrations between the different CO_2 treatments. DIC concentrations of those mesosoms that were initially exposed to high CO_2 (DIC) concentrations are "offset"-corrected so that their initial mean DIC matches the initial mean of the present day DIC concentrations. Mesocosms

of the low CO_2 treatment were adjusted likewise. In this manner, all initial mean DIC concentrations have become identical, but changes and variations (between the mesocosms) with respect to these mean values remain. Thus, variances of the respective LC, MC, and HC mesocosms can be calculated after applying these (two) offset corrections to all DIC data of the high- and low CO_2 treatements. Eventually, individual standard errors for the LC, MC, and HC mesocosms are derived for all sampling dates.

The time-varying covariance matrices $\mathbf{R}_i$ are constructed with $\mathbf{S}_i$ (with diagonal elements of standard errors, see Eq. B.3 in Appendix B) together with some correlation matrices ($\mathbf{C}_{(\boldsymbol{y})}$). Correlations between measurements were computed based on data of all nine mesocosms. Two matrices $\mathbf{C}_{(\boldsymbol{y})}$ have been derived from data for two distinct periods: 1) the exponential growth phase, and 2) the post-bloom period.

$$\mathbf{R}_i = \mathbf{S}_i \cdot \mathbf{C}_{(\boldsymbol{y})} \cdot \mathbf{S}_i \tag{7}$$

Equation (7) is applied because correlations between observations can change from pre-bloom period to post-bloom period. For example, PON and DIC are strongly negatively correlated during the exponential growth phase but become weakly positively correlated during the post-bloom period, when both, DIC and PON, decrease. The correlation matrices, $\mathbf{C}_{(\boldsymbol{y})}$, for the two respective periods are also given in the Appendix (B).

A maximum likelihood (ML) estimator is applied, meaning that no explicit prior information is considered for the estimation of parameter values. Eventually, we use three similar cost functions but with data ($\boldsymbol{y}$) and covariances ($\mathbf{R}$) from the respective three mesocosms of each case. These daily data ($\boldsymbol{y}_i$) are available for a period of $N_t = 23$ days, with subscript i indicating the day when measurements were made. The elements of the parameter vector of interest (Θ) are those parameters listed in Table (1), including the initial value of PON_0 and initial condition parameters that further specify how PON_0 is distributed between detritus, zooplankton, coccolithophores and the remaining photoautotrophs. For a maximum likelihood (ML) estimation of the parameters (including the initial conditions) we maximise the conditional probability of explaining the data given our model together with a set of values assigned to the parameters (to each element of Θ):

$$p(\boldsymbol{y}|\Theta) = \text{constant} \cdot \exp[-\frac{1}{2}\sum_{i=1}^{N_t} \boldsymbol{d}_i^T \mathbf{R}_i^{-1} \boldsymbol{d}_i] \propto \exp[-\frac{1}{2}J(\Theta)] \tag{8}$$

The ML estimate of parameter values can be found by actually identifying the minimum of the exponent of $p(\boldsymbol{y}|\Theta)$ of Eq. (8), since the constant term is independent of Θ. We thus compute and minimise the following cost function $J(\Theta)$:

$$J(\Theta) = \sum_{i=1}^{N_t} (\boldsymbol{y}_i - H_i(\boldsymbol{x}))^T \mathbf{R}_i^{-1} (\boldsymbol{y}_i - H_i(\boldsymbol{x})) \tag{9}$$

We not only wish to identify the minimum of $J(\Theta)$ that corresponds with one best estimate of parameter values ($\widehat{\Theta}$) but also confine a credible region of parameter estimates. This credible region tells us how reliable the parameter estimates are (yielding lower and upper credibility limits) and resolves correlations (collinearities) between the parameters. The parameter optimisation procedure implemented in this study is described in detail in the Appendix (B).

3 Results

3.1 Parameter estimates for specific mesocosms with low, medium, and high calcification

The same seven model parameters (Table 1) were optimised for all three calcification cases (LC, MC, and HC) independently, using data from respective mesocosms. With our data assimilation approach we can thus specify commonalities and differences between model solutions for mesocosms with LC, MC and HC. Table (2) lists all ML estimates, which correspond with the best model solutions obtained with the Markov Chain Monte Carlo (MCMC) method. Collinearities are expressed by the correlation coefficients of two parameter combinations, which we have also calculated based on results of the MCMC method (Table 3).

Credible intervals limits for each parameter were derived from nonparametric probability densities of the MCMC estimates. The figure (4) shows cumulative density function (CDF) for corresponding posterior probability distributions. The steeper the CDF increase the narrower the 95% credible interval of the parameter estimate. According to the width of credible intervals we find uncertainty ranges of initial conditions parameters f_{det}, f_{zoo} and PON_0 to be generally small for all three cases of calcification respectively. The initial condition parameters are best constrained for the solution of medium calcification (MC). The parameter f_{cocco} shows the largest uncertainty for the HC case. A large fraction (≈ 90 %) of initial biomass comprises of detrital matter in all three solutions. Table (4) shows mean concentration values of PON_0, $DetN_0$, $ZooN_0$, $CoccoN_0$ and $PhyN_0$ along with their uncertainties according to respective MCMC estimates. Initial zooplankton concentration is highest in HC solutions. Thus, more photoautotrophic biomass is lost due to grazing by zooplankton and less by aggregation in model solutions for HC, which is reflected by the negative correlation between initial condition parameters f_{zoo} and f_{det}. For those parameters that do not specify the initial conditions we hoped to find all credible intervals to overlap, which would have suggested insignificant differences between the estimates. A single set of values of these parameters could then be unambiguously used for simulations of all nine mesocosms, independently of how the values of the initial conditions turned out to be. This is not the case, as can be seen in Fig. (4) and in the correlation coefficients (Table 3). Estimates of the subsistence quota (Q_0) are lower for the mesocosms with high and medium calcification rates. Apparently, lower Q_0 and higher α_{cocco} values are required to buildup high coccolithophores biomass in mesocosms with high calcification rates as initial coccolithophores concentration is low and grazing pressure is high.

During the post-bloom period, the mesocosms pooled in HC reveal TA changes that are consistently higher than in the LC mesocosms. In fact, these differences become well reflected in our parameter estimates. Thus, our optimised ensemble model solutions are providing the statistical evidence that HC and LC are significantly different. With respect to the mesocosms assigned to the MC (medium calcification) case we see in our parameter estimates and ensemble model solutions that they are rather close to conditions also met by the HC mesocosms. In this case the differences in parameter estimates (between MC and HC) are small, although we find significantly different estimates for α_{cocco} and for f_{zoo} between MC and HC (see Fig. 4). Thus, we may have one or two out of the three MC mesocosms that might have been better assigned to the HC case. However, this is reflected in our data assimilation results and we are primary concerned with the upper and lower extremes in calcification, as resolved by the six mesocosms in the LC and HC cases.

3.2 Data-model comparison

The variational range of parameter estimates (Fig. 4) induce ensembles of model trajectories (model results) that are statistically indistinguishable (or equivalent). Based on these posterior ensemble parameter estimates of all three calcification solutions we find a general good agreement between model results and the data, (Fig. 5).

The ensembles reflect uncertainty ranges in model solutions, which correspond nicely with most of the variability in obser­vations. Almost the entire range of variability in TA is recovered with our three distinct solutions of calcification. The observed variability in POC is captured with the optimal ensemble model solutions. Only few maximum values seen in POC data remain unresolved, likely because we have optimised parameters that hardly introduce changes in the solution of TEPC concentrations. The model solutions exhibit some faster increase in the accumulation of PON during the exponential growth phase, in spite the fact that DIN data are matched well. Although this systematic model offset (bias) is pronounced, it does not correspond with any similar model bias in POC. Another general offset can be seen for simulated Chl a concentrations during the post-bloom period. Our model shows sharp draw down in Chl a in all three solutions (HC, MC and LC) during the post-bloom period, whereas observed Chl a values are more variable.

3.2.1 Variations in calcification in response to growth conditions

According to our model approach we resolve changes in the rate of calcification relative to the carbon that is assimilated for growth of the coccolithophores. For the period of nutrient repletion the values of the molar calcification-to-C-assimilation ratio (ΔPIC : ΔC ≈ 0.5) are smaller than the values under nutrient depleted growth conditions. All ensembles of model solutions (LC, MC, and HC) reveal a similar behaviour, with variations in ΔPIC : ΔC greater than 0.5 (up to 2.2) for growth rates between 0 and 0.3 d^{-1}. These variations depend on the light-acclimation state (e.g. θ_{cocco}), fluctuations in irradiance and on cell quota (Q^N_{cocco}). The variations in ΔPIC : ΔC during nutrient depleted period can be attributed to fluctuations in carbon assimilation due to production of TEPC .

3.2.2 Distinctions between model results of low, and high calcification (LC and HC)

Optimised model results of low calcification (LC) yield the highest TA values of all mesocosms, being in accordance with the TA data. DIN concentrations are well resolved by the model and variations of the ensemble DIN simulations are similarly low as in observations. The previously mentioned biases in PON and Chl a are most conspicuous in this LC ensemble of optimal model results. Variability in the POC data of the LC mesocosms is not captured by the model ensemble. But simulation results (solid lines in Fig. 7) match the POC mean of the three mesocosms. For PIC we also find a good agreement between model ensemble results and data. However, a noticeable potential bias exists for the PIC response in the high CO$_2$ treatment (M1), where model results overestimate PIC data during the maximum bloom period and shortly after nutrient depletion. This overestimation is more pronounced in mesocosm with high CO$_2$ treatment. The LC ensemble successfully reproduces amplitude of Chl a peak seen in data, this is also the case in the solutions of HC mesocosms.

DIN (dissolved inorganic nitrate) is well resolved in the HC (high calcification) solutions (Fig. 8). Simulated Chl *a* also fits well to observations. HC solutions yield largest variability in DIC, TA and PIC amongst all optimised solutions, which we mainly attribute to the large uncertainty ranges of the model parameters f_{cocco} and α_{cocco}. The HC solutions show sharp drawdown in DIC during the bloom period compared to other solution (LC). This can be explained by an enhanced calcification

5 activity due to high growth rates of coccolithophores in HC during the bloom period. Again, model overestimates observed PIC values (M3) under high CO_2 conditions shortly after the maximum of bloom. PON is best reproduced in this HC case in comparison to LC. Although model's HC solutions reproduce the entire variability in observed PIC, the corresponding best fits (to M3, M4, M9) underestimate PIC data.

3.2.3   Integrated flux estimates of carbon and nitrogen (C and N budgets of mesocosms)

10 The ensemble model solutions for LC and HC constitute two extremes and we therefore concentrate on the C and N budgets of these two cases. Carbon and N flux estimates were computed as integrals over the entire 23 days period. Figure (9) show mean C and N flux estimates and their standard errors of the LC solutions of the low and high CO_2 treatments. Figure (10) shows the corresponding flux estimates for the HC solution. We learn from these flux estimates that the simulated C and N mass flux estimates differ more between the mesocosms with different calcification rates than between the mesocosms exposed

15 to different CO_2 levels. In both cases (LC and HC) most inorganic carbon and nitrogen (DIC and DIN) are utilised by non-calcifiers (≈ 56 % in case of HC and ≈ 64 % in the LC solution), despite the differences between LC and HC. Generally, more carbon fixation (with C:N uptake ratio of $168:10 \approx 17$) occurs in the HC than in the LC mesocosms (C:N uptake ratio $\approx$ 13). Flux budgets show that non-calcifiers clearly dominate in mesocosms with low calcification rates, and in HC mesocosms coccolithophores and bulk phytoplankton biomasses are comparable (Figs. 9 and 10). Although grazing, in general, is high in

20 HC mesocosms (Table 4), there is a trend of higher grazing pressure on bulk phytoplankton than on coccolithophores. This is shown by N flux estimates, where zooplankton gain nearly 57% of their total biomass through grazing on non-calcifiers in HC and LC. According to our model solutions, the coccolithophores are always less vulnerable to grazing than the bulk phytoplankton. This model behaviour may not be fully conclusive, because we have no information about the actual grazing rates or about grazing preferences. A noticeable difference between high and low calcification model ensembles is in terms

25 of mortality of zooplankton. Higher mortality is seen in HC solutions. Since the carbon fixation in HC is high, exudation and leakage rates are also higher. Accordingly, TEPC production is enhanced in HC solutions. Unlike estimates of C flux, the N fluxes in HC and LC ensembles are similar, e.g. aggregation losses of phytoplankton and of coccolithophores are 3 ± 0.4 and 2 ± 0.4 mmol N m^{-3} in HC, and $3.4 \pm 2 \cdot 10^{-3}$ and $1.5 \pm 2 \cdot 10^{-3}$ mmol N m^{-3} in LC respectively. Similarly, flux estimates of all mesocosms show almost same rates of DIN utilisation, excretion, exudation and remineralisation.

30 ## 4   Discussion

The data assimilation approach applied in this study was designed to resolve differences in TA and thus in calcification, while variations in other data (e.g. DIN, PON, and POC) should also be explained with our model. We distinguished between meso-

cosms with high, medium and low calcification rates (HC, MC, and LC) and their respective data were used to come up with optimal estimates of initial conditions and of some important physiological model parameters. Ideally, we would have identified similar optimal values of the physiological parameters and would have obtained different estimates of the initial conditions for all three cases, HC, MC and LC respectively. However, our results reflect a more complex picture and our optimised values for the initial conditions also depend on the best estimates for the model parameters. The initial conditions could not be constrained independently and model solutions of the HC case do not automatically imply a higher initial abundance of coccolithophores relative to the other, non-calcifying, phytoplankton. Likewise, the LC solution does not require a lower initial biomass of calcifying algae. Instead of differences in relative species abundance, the initial physiological conditioning, e.g. acclimation states of the algae, seems relevant as well, which is in the end reflected in the estimates of the physiological parameters Q_0, α_{cocco}, and α_{phy}). An alternative data assimilation approach would be to optimise the physiological model parameters (Q_0, α_{cocco}, and α_{phy}) together with the initial conditions (PON_0, f_{det}, f_{zoo}, and f_{cocco}) for mesocosms of one calcification case in a first step, e.g. the MC case (using data of mesocosms M2, M5, M7). In a second step we could have fixed the optimised physiological model parameters Q_0, α_{cocco}, and α_{phy} (as identified with data of e.g. the MC case) and would have then estimated only the initial condition parameters for the other mesocosms, e.g. low and high calcification (LC and HC). This alternative approach does work (not shown), but we learned that we may then put too much confidence into those estimates of Q_0, α_{cocco}, and α_{phy} obtained first, e.g. estimates for the MC mesocosms. It can even obscure the fact that collinearities exist between some initial condition estimates and the other model parameters. Furthermore, with such alternative approach we could end up with different estimates of the initial conditions, if we would have started with data of either the HC or LC mesocosms first instead. The design of our data assimilation approach is more challenging but it is better suited to disclose major uncertainties and collinearities in estimating initial conditions together with model parameters of algal growth.

4.1 Uncertainty ranges in parameter estimates and variability in model solutions

Large variations can be seen in the data of PIC, reflecting the variability measured in TA. Since optimal ensembles of model solutions were derived for three distinct cases of calcification (LC, MC and HC), we automatically capture most of the observed variability in PIC with our simulations. The spread of the ensemble solutions for TA and PIC is smaller in each of the three cases relative to the observed total range. This means that the respective uncertainties in our parameter estimates are small enough to obtain three distinctive ensembles of model solutions. However, as discussed before, it is not possible to identify optimal values of the initial condition parameter f_{cocco} independently from estimates of the other physiological model parameters. This situation is aggrevating but not unusual (Schartau et al., 2016). For instance, in a sensitivity study with a regional marine ecosystem model Gibson and Spitz (2011) stressed that collinearities exist between initial conditions and the values assigned to the biological parameters.

The posterior uncertainties in the estimates of the subsistence quota, (Q_0), are rather small, if compared with the uncertainty ranges of the other parameter estimates. Likewise, parameter estimates of the initial condition parameters PON_0, f_{det}, and f_{zoo} are fairly confined. The variational range that we see in our model solutions is mainly induced by uncertainties in estimates of the photosynthesis parameters α_{cocco}, α_{phy} and of f_{cocco}. The combination of these three parameters mainly determine the

spread in model solutions with respect to the amount of C-fixation and also calcification. This also explains why the ensemble model solutions exhibit only small variations in DIN and PON concentrations and thus in our N-flux estimates.

Variability in POC is much more pronounced than in PON. All three model solutions show a steep increase in POC:PON ratio as soon as algal growth becomes nutrient limited (Fig. 11). The variability seen in the POC:PON ratio is thus mainly due to a temporal variation in Q^N (N:C ratio of both photoautotrophs) and thus of the algal growth conditions. The temporal variations in Q^N eventually disperse into zooplankton biomass and detritus, inducing elevations of their respective C:N ratios during the post bloom period. Another contribution to the elevation of POC:PON ratios is also related to changes in POC because it constitutes concentrations of TEPC, which is explicitly resolved in our model.

Our results show an increase in molar ΔPIC : ΔC-assimilation at low net growth rates (μ_{cocco}) under nutrient limited conditions (Fig. 6) in both HC and LC cases. These variations are translated in to some variability seen in the PIC:POC ratio. Variability in PIC:POC is discussed in Engel et al. (2014), where they collected and analysed data of diverse experiments and documented an increase (up to fourfolds) in values of cellular PIC:POC at relative growth rate (RGR) ≈ 0.2 d^{-1} and below in various CO_2 treatments. The reason for a sharp increase in molar ΔPIC:ΔC-assimilation ratio at low growth rates in our model is because of a down regulation of light harvesting complex (LHC). Such model behaviour is in agreement with the interpretation of Barcelos e Ramos et al. (2012), who describe calcification as a process into which the coccolithophores can channel excess energy. In order to maximise (optimise) growth rate under nutrient depleted and high light conditions, the model allocates more resources and energy to support nutrient acquisition than to the light harvesting complex (indicated by low $f0_{cocco}^{LHC}$ values). Since ΔPIC:ΔC-assimilation is inversely related to $f0_{cocco}^{LHC}$ in our model, an increase in calcification (relative to C-fixation) is obtained at low growth rates. The maximum of ΔPIC:ΔC-assimilation ratio in our simulations are in accordance with those found in Barcelos e Ramos et al. (2010).

4.1.1 Differences between high and low calcification solutions (HC and LC)

The optimised model solutions for HC and LC reveal significant differences in the development of coccolithophore biomass. As discussed before, these differences are not solely attributable to differences in the relative proportions of initial biomass concentrations. In fact, the optimisations yielded estimates that suggest fairly similar initial coccolithophore biomass concentrations between all nine mesocosms. Eggers et al. (2014) stressed that variations in initial plankton composition can be responsible for large differences in the responses observed on community level, thereby masking any possible CO_2 effect on photosynthesis or calcification. Briefly, our results not only support the findings of Eggers et al. (2014), they provide additional insight to the problem of resolving a CO_2 response in the presence of variability in measurements. One added message compared to Eggers et al. (2014) is that our mass flux estimates are shown to differ more between the different calcification solutions than between the different CO_2 treatments. This situation exemplifies that simulation results (e.g. future model projections) may involve uncertainties in flux estimates that are larger than the CO_2 effect introduced to the model (e.g. by following Findlay et al., 2011). Another added message is that initial conditions may not be independently estimated from estimates of phytoplankton growth parameters, like α_{phy} and α_{cocco}. This is particularly relevant for model assessment and model analyses of mesocosm experiments. We stress that the original design of the experiment was meaningful, in particular with respect to the initial filling

of the mesocosms in the PeECE-I experiment. The retrospective separation of the CO_2 response signal from the system's variability was only possible because mesocosms with similar initial conditions were subject to different CO_2 concentrations. Such separation would be more difficult in retrospective if mesocosms with similar initial conditions would have been (by chance) exposed to similar CO_2 levels.

From a modelling perspective it is helpful to know about the initial individual mass contributions to PON_0, including details in the initial composition of the plankton. But the level of compositional detail remains unclear, since these variations in individual plankton composition will in the end always translate into some variational (uncertainty) range in e.g. the initial photo-acclimation state, since our model approach only distinguishes between calcifiers and all other, non-calcifying, phytoplankton. These considerations were disregarded when we designed this study and we originally thought of the importance of the relative mass distributions between the state variables resolved by our model, while imposing fixed initial stoichiometric ratios (C:N and Chl$a$:N). It seems plausible to allow for some variations of the initial stoichiometric ratios as well.

For now we are interested in the question: what induces the different model solutions for LC and HC, in spite of similar initial conditions in the concentrations of coccolithophores and phytoplankton? First of all, we have some differences between the relative proportions of initial detrital, zooplankton, and photoautotrophic biomass (e.g. DetN:ZooN:(PhyN+CoccoN) = 80:10:1 for HC and 28:3:1 for LC). The difference between these ratios point towards net photoautotrophic growth rates that are higher in the LC case than in the HC case, since losses due to grazing and aggregation must be lower in the LC case. However, the initial conditions in mesocosms of the LC case do not automatically yield model solutions of highest photoautotrophic growth. Instead we find overall reduced growth rates but some pronounced differences in the relative proportions of biomass between the coccolithophores and the non-calcifying phytoplankton (Fig. 12). The reason for these differences lies primarily in the relative differences between the estimates of the physiological parameters, with estimates of α_{cocco} being always smaller than of α_{phy}. The photosynthetic efficiency of the coccolithophores remains clearly smaller (LC case) or can become similar (HC case) relative to the other, non-calcifying, phytoplankton. Major differences between the LC and HC solutions can thus be attributed to higher α_{cocco} values (median α_{cocco} = 1.7 mol C (g Chl a)$^{-1}$ m^2 W^{-1} d^{-1}) in HC posterior distribution compared to LC (median α_{cocco} = 1.4 mol C (g Chl a)$^{-1}$ m^2 W^{-1} d^{-1}). The estimates of α_{cocco} are negatively correlated with the estimates of f_{cocco} (Table 4) and we may therefore look on the combination of the two parameters. To do so we compare two extreme solutions, selected from the ensemble solutions of LC and HC respectively. One extreme solution yields the lowest calcification among all HC solutions, based on the parameter combination (α_{cocco} = 1.84 mol C (g Chl a)$^{-1}$ m^2 W^{-1} d^{-1}, f_{cocco} = 0.34). The other selected solution represents the highest calcification of all LC solutions, which corresponds with (α_{cocco} = 1.59 mol C (g Chl a)$^{-1}$ m^2 W^{-1} d^{-1}, f_{cocco} = 0.35). Thus, it is mainly the photosynthetic efficiency α_{cocco} to which the model solution is highly sensitive to. Hence, a difference of ≈ 0.3 mol C (g Chl a)$^{-1}$ m^2 W^{-1} d^{-1} can effectively determine the differences in our simulations with respect to rates of carbon fixation and calcification. The build-up of comparable nitrogen biomass of coccolithophores and bulk phytoplankton in HC solutions are achieved with identical Q_0 values and only nuanced differences in values between α_{cocco} and α_{phy}. In contrast, bulk phytoplankton (non-calcifiers) outcompete coccolithophores during the bloom period in the LC solutions (Fig. 12).

Differences in photosynthetic efficiency estimates for the LC and HC cases could possibly be invoked for two reasons: a) because of unresolved differences in initial photo-acclimation states (e.g. different light-history during the filling period), since we assume identical initial Chl:N ($\theta_{cocco}^N = \theta_{phy}^N$) and N:C ($Q_{cocco} = Q_{phy}$) ratios for all nine mesocosms (and thus for LC, MC, and HC), or b) because of unresolved varying conditions in irradiance. To impose identical surface PAR forcing on all nine mesocosms might not be appropriate and the arrangement of neighbouring mesocosms may have caused some shading effects. From the available data and with our model approach it is not possible to resolve such varying conditions afterwards.

4.2 Model biases

Model biases disclose systematic deviations of simulation results from observations, which may point towards i) erroneous model counterparts to observations (definition of $H(\boldsymbol{x})$ in Eq. 9) or ii) deficiencies in model dynamics (errors in $\boldsymbol{x}$). Some bias is related to the increase in PON concentration during the late phase of exponential growth (between days 10 and 12, Fig. 12). The noticeable bias (temporal offset) in simulated PON concentrations can be explained with an apparent overestimation of initial coccolithophore biomass. The estimates of f_{cocco} turned out to be highest, if compared with the estimates for the low and high calcification (LC and HC) model solutions. Furthermore, the range of credible values for f_{cocco} is small (Fig. 4). Both estimates, of f_{cocco} and of PON_0, lead to an inital biomass concentration of coccolithophores that is approximately three times higher than in the LC case and even six times the initial concentration of the model solutions for HC.

With our model we do not distinguish between growth of picoplankton and the other non-calcifying phytoplankton during the initial bloom phase. The initial abundance of picoplankton (mainly *Micromonas spp.*) and their decline was observed during the early pre-bloom period of the PeECE-I experiment (Engel et al., 2005). This explains why our simulated Chl *a* and PON concentrations are lower compared to observations between day 1 and day 4. Another discrepancy between simulated and observed Chl *a* exists during the post-bloom period. We assume that this bias is mainly because we do not account for detrital chlorophyll pigments (presumably of inactive or destroyed cells) in our model. Formation of detritus is associated with the aggregation of coccolithophores and of the other phytoplankton to form detritus (simulated as a transfer of algal biomass into detritus) in our model, and the fate of Chl *a* within the detritus compartment remains unresolved. Once N and C biomass of the photoautotrophs are transformed to detritus, an associated flux of Chl *a* is disregarded. An explicit consideration of the fate of Chl *a* would likely improve model performance and some refinements in this respect are recommended for the future.

Results of our data-model synthesis also exhibit a small but distinctive bias in the calcification response to elevated CO2 levels. The distinctions we made with respect to mesocosms of LC, MC and HC helped us to identify such bias. This bias implies that the CO_2 effect on calcification, as introduced to our model, is slightly smaller than in the observations, which will be discussed in detail hereafter.

4.3 Disentangling CO$_2$ effect from the observed variability in PIC

We considered a simple CO_2 relationship that mimics only OA effects on calcification. It is a dependency that was adopted from the meta-analysis of Findlay et al. (2011). With this CO_2 dependence we can already capture differences in PIC formation. The CO_2 sensitivity that we introduced to our model is only effective with respect to the ratio of calcification versus C-fixation,

thereby reducing the overall calcification rate under high CO_2 conditions. This effect turned out to be small compared to the total variability seen in PIC data. According to our model setup we do not consider any potential changes in vulnerability to predation (or edibility) of the coccolithophores due to elevated CO_2. Likewise, any additional CO_2 effects, e.g. on the rate of aggregation, are not accounted for. Such effects remain unresolved and therefore the comparison of our budget calculations

5 yield only small differences between high and low CO_2 levels, in particular with respect to nitrogen flux estimates. Thus, differences in C and N budgets between the two extreme calcification cases, LC and HC, are more pronounced than between different levels of CO_2. To resolve consecutive ecological effects in response to a reduction of the relative calcification rate we would have needed explicit data, i.e. revealing differences in grazing and aggregation rates between the individual mesocosms. With the PON and POC data used in our data assimilation approach it is not possible to distinguish between different coccol-

10 ithophore loss terms like grazing and aggregation, since detritus and zooplankton are both constituents of the same PON and POC measurements.

The advantage of resolving LC, MC and HC solutions separately is that for each case we can compare data with model results of mesocosms individually, of low (glacial), medium (present), and high (future) CO_2 treatments. In other words, for every LC, MC, and HC case we resolve three mesocosms, of which each was subject to different CO_2 levels. This way we have

15 separated differences between LC, MC, and HC from variations induced by a CO_2 effect. Doing so reveals PIC formation to be be systematically overestimated by the model for all mesocosms of the future treatment (Figs. 7 and 8, MC case not shown). In contrast to Delille et al. (2005), our results show an early onset of calcification in mesocosms of the high CO_2 treatment between day 10 and day 15. It indicates that the CO_2 effect introduced to our model is likely too weak. This becomes evident according to positive model-data residuals in PIC between day 13 and day 18 for those mesocosms with future treatment (Fig.

20 13). It is not evident for the glacial and present day CO_2 treatments, where the corresponding residuals do not show a systematic positive offset.

Figure (14) shows the total variability seen in PIC data together with the full variational range of all ensemble model solutions. In addition, we depict those ranges in simulated PIC that are solely due to the CO_2 effect, based on the two extreme calcification solutions (lowest and highest simulated PIC) and the best model solution (according to the lowest cost function

25 values) for the MC mesocosms. If we compare the simulated CO_2 response signal on calcification with the total variability in PIC (in Fig. 14) we find that the CO_2 effect remains small. This situation demonstrates the difficulty in isolating a distinctive CO_2 signal from the total variability seen in PIC observations. However, with our model-based analysis approach this CO_2 signal becomes well detectable.

5 Conclusions

30 An analysis of data of a mesocosm experiment is often approached by first grouping individual mesocosms according to the level of perturbation (e.g. the level of DIC added). In some cases, such apparently self-evident approach may not help to reveal some basic phenomenon in mesocosm experiments. For a meaningful data analysis the mesocosms need not be exclusively differentiated by the different levels of perturbation but may first be sorted by major differences between relevant response

signals, as done with respect to the magnitude of calcification in our study (by differentiating between LC, MC, and HC). In mesocosm experiments these differences in responses are likely associated with variations in initial conditions.

With our data assimilation approach we could disentangle three distinctive ensembles of model solutions that represent mesocosms with high, medium and low calcification rates. The results of our data-model synthesis show that the initial relative abundance of coccolithophores and the prevailing physiological acclimation states drive the bloom development and determine the amount of calcification in the mesocosms. Small variations of these two initial factors between the mesocosms can generate differences in calcification that are larger than the change in calcification induced by OA. In spite of this difficulty, a CO_2 response signal may still be identifiable, as long as mesocosms that reveal strongest similarities (with respect to initial composition of plankton and their physiological state) are not used as replicates for similar CO_2 conditions (perturbations). Instead, mesocosms with similar initial conditions should be exposed to different levels of OA. Such favourable starting conditions were met in the mesocosm experiment described in Engel et al. (2005) and Delille et al. (2005), as well as in the experiment of Eggers et al. (2014).

An alternative approach to setting up mesocosms is to gradually increase the level of perturbation for a series of mesocosms. This way a gradient of different perturbation levels is introduced. The advantage then is that mesocosms that have been collated according to e.g. lowest and highest response signals (or likewise according to similarities in initial conditions) may then be separately analysed with respect to their responses to the individual levels of perturbation.

From this modelling study we infer that collinearities exist between estimates of initial conditions and physiological model parameters, in particular for the photosynthetic efficiencies α_{phy}, α_{cocco} and the initial fraction of coccolithophores determined by f_{cocco}. Therefore, it is not possible to identify initial concentration of photoautotrophs independently of parameters responsible for phytoplankton growth in HC, MC and LC model solutions. This was only found because we optimised initial conditions together with physiological parameters for HC, MC and LC mesocosms separately. By this seperation we could better specify the CO_2 effect on PIC formation. Doing so we could identify a systematic overestimation of calcification in our model and we conclude that our simulated CO_2 effect on PIC formation is even too weak.

Acknowledgements. The development of the modelling framework for mesocosm simulations and data assimilation was supported by the large integrated project Surface Ocean Processes in the Anthropocene (SOPRAN, 03F0662A), funded by the German Federal Ministry of Education and Research (BMBF). This study is a contribution to the BMBF funded BIOACID (03F0728A) project. We gratefully acknowledge support by Markus Pahlow, who helped to refine equations in our model. We also like to acknowledge support given by Andreas Oschlies and by the GEOMAR data management team. We thank Sabine Mathesius for the compilation and inclusion of the forcing data into the mesocosm modelling setup. We thank Yonss Jose and Hadi Bordbar for helpful and constructive comments.

6 Figures
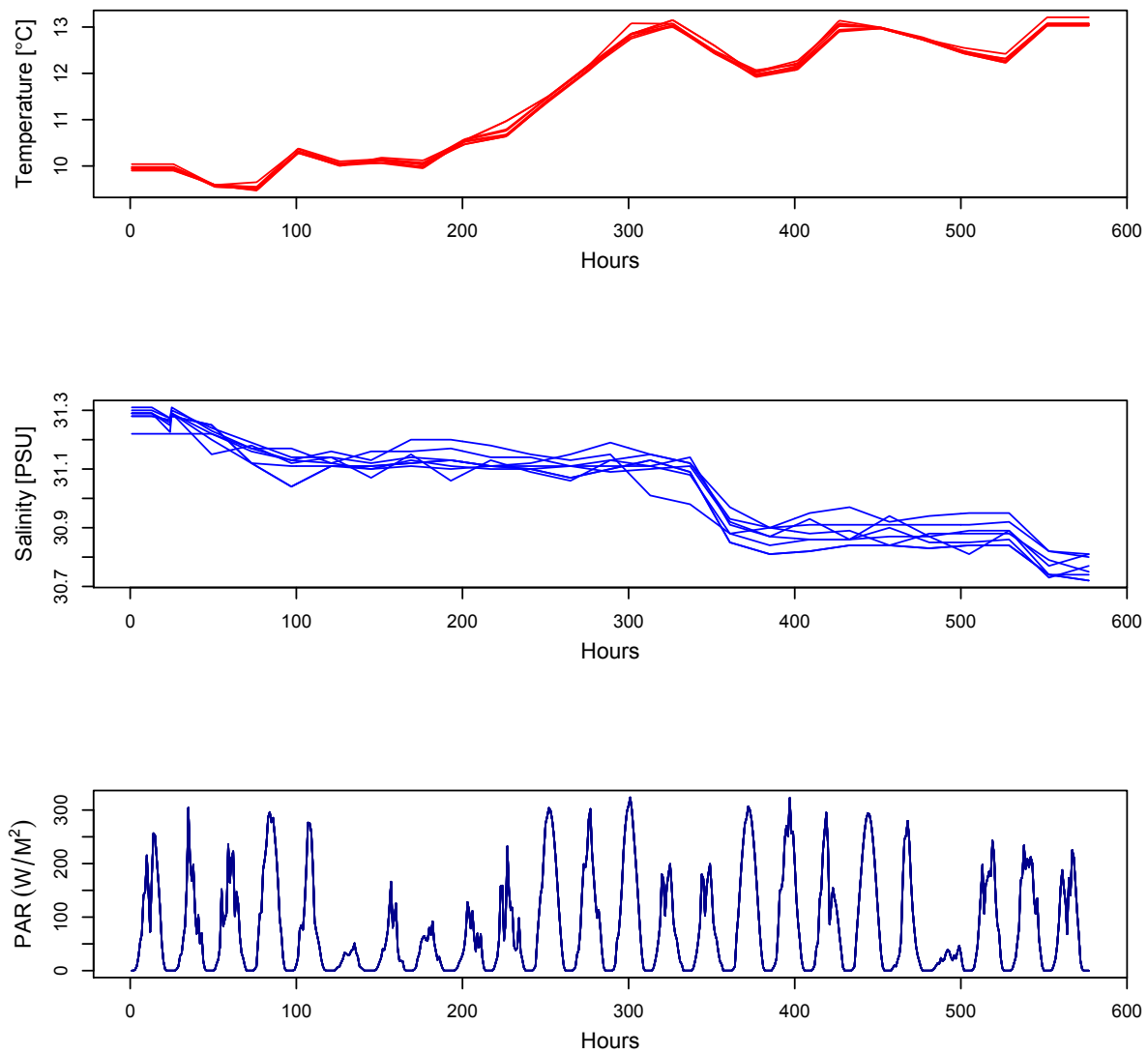
Figure 1. Forcing variables for all nine mesocosms: The upper panel shows temperature, linearly interpolated to hourly values between daily observations. The middle panel displays hourly interpolated salinity values and the lower panel reveals the irradiance data with hourly temporal variations resolved.
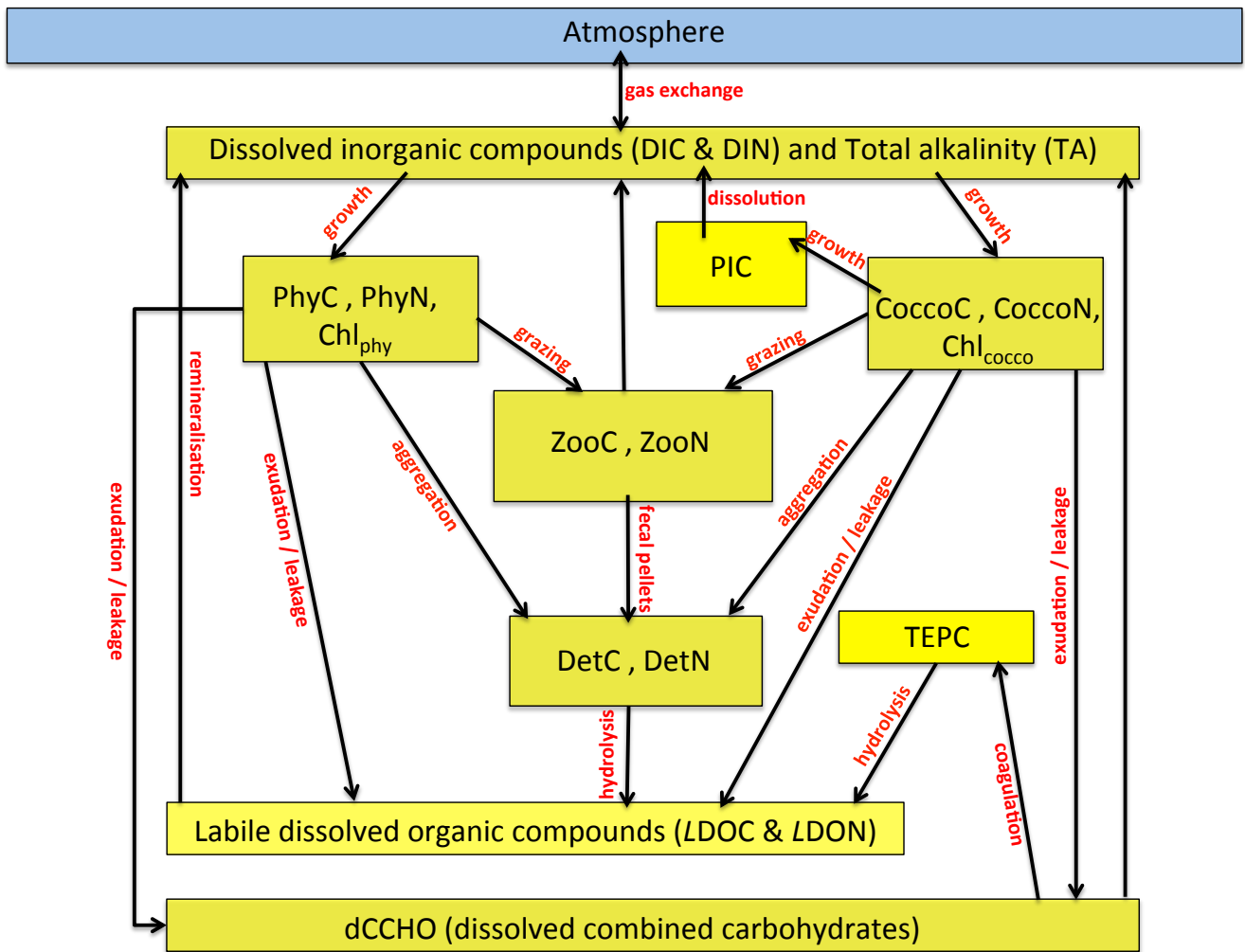
Figure 2. Schematic representation of the model: boxes characterise individual compartments that are represented by one and more model state variable. The arrows represent key biogeochemical processes (named in red) between compartments. One compartment includes dissolved inorganic carbon and nitrogen (DIC and DIN). This comartment also embeds total alkalinity (TA). Biomass and chlorophyll concentrations of photoautotrophs are resolved with respect to carbon and nitrogen explicitly (referred to as PhyC and CoccoC, PhyN and CoccoN, and Chl$_{phy}$ and Chl$_{cocco}$ respectively). Variations in carbon and nitrogen biomass are also resolved for zooplankton (ZooC and ZooN) and for detritus (DetC and DetN). Dissolved combined carbohydrates (dCCHO) are distinguished from other labile dissolved organic matter, desribed as *L*DOC and *L*DON. Only dCCHO are assumed to act as precursor for the formation of transparent exopolymer particles, whose carbon content is explicitly resolved (TEPC). One compartment represent the formation and dissolution of particulate inorganic carbon (PIC), affecting DIC as well as TA.
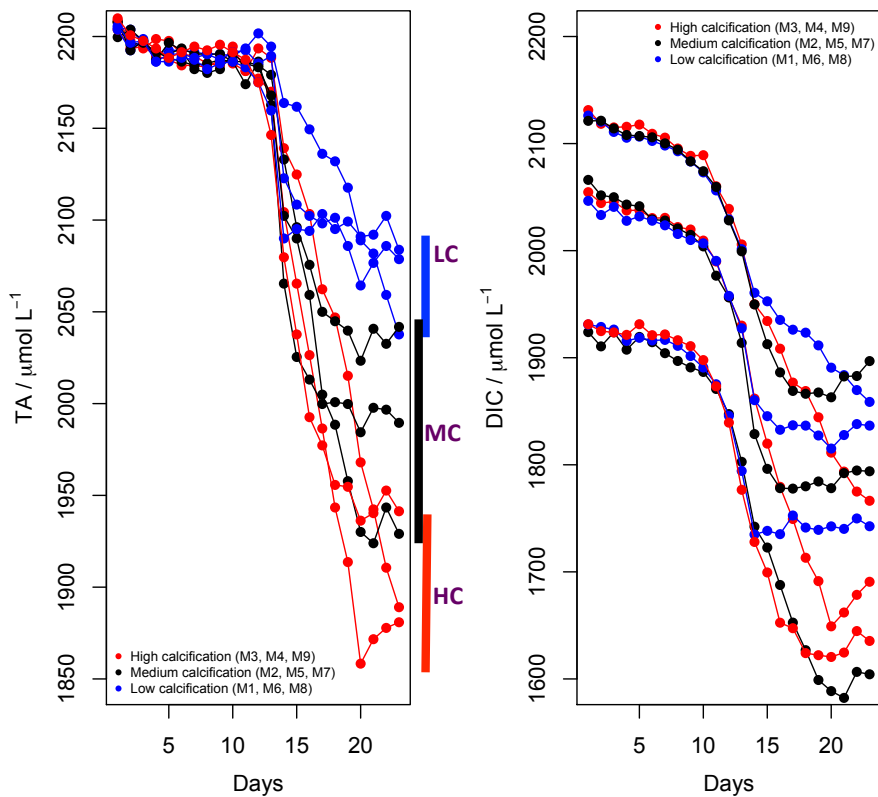
Figure 3. The left panel in the figure shows three distinct calcification patterns, reflected in total alkalinity (TA) data. Those mesocosms that exhibit high TA values (a reduced drawdown during the bloom and post-bloom period) feature rates of low calcification (LC, in blue color). Mesocosms with low TA values (a strong reduction of TA) reveal rates of high calcification (HC, marked red). Rates of medium calcification (MC) are assigned to the remaining mesocosms (with intermediate TA values, marked black). The right panel shows the respective different CO_2 treatments in the same colors as for LC, MC, and HC. The figure shows that each calcification case (LC, MC, and HC) includes mesocosm of all three CO_2 treatments.
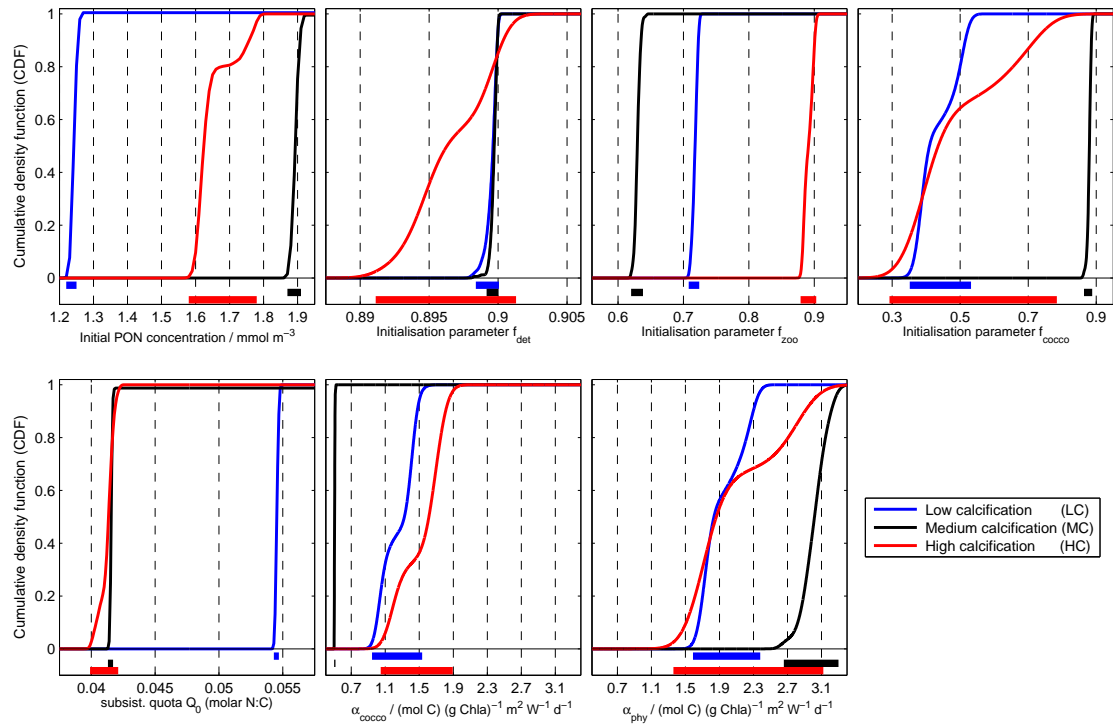
Figure 4. Probability distributions of the initial condition and physiological model parameters: the cumulative sum of non-parametric probability densities (CDF) were derived from the posteriors of the Markov Chain Monte Carlo (MCMC) approach. The bars on the bottom of each panels show respective 95% credible (uncertainty) ranges of the parameter estimates.
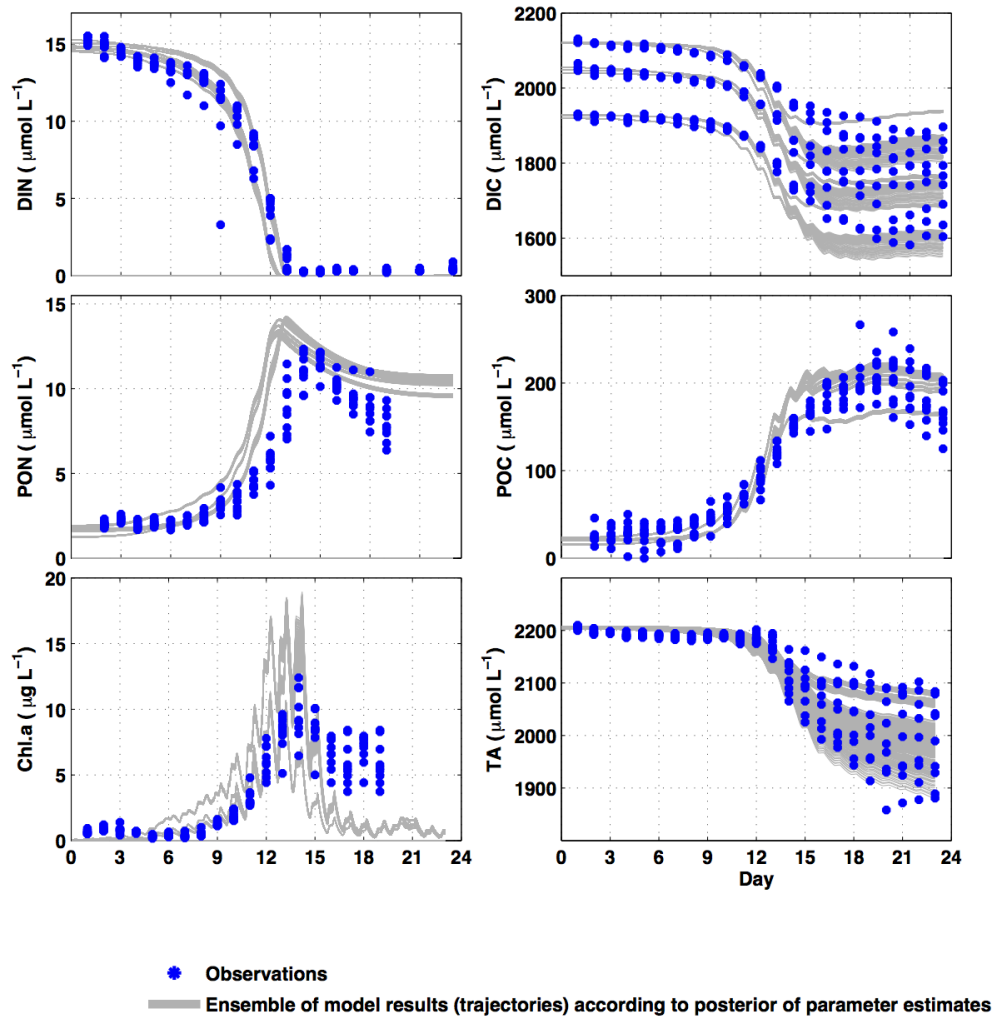
Figure 5. Full variational range of model outputs due to uncertainties in parameter estimates. Model ensembles of high, medium and low calcification solutions compared with observations.
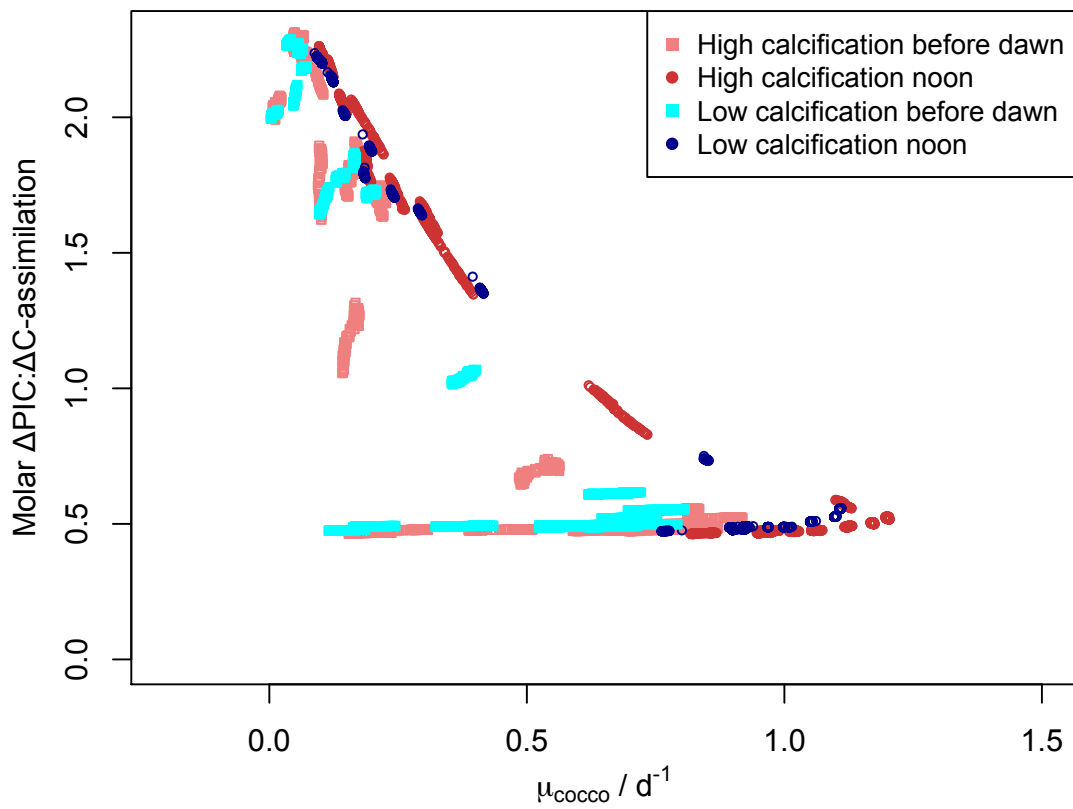
Figure 6. Molar calcification-to-C-fixation ratio compared to net growth rate of coccos (μ_{cocco}) in high and low calcification solutions.
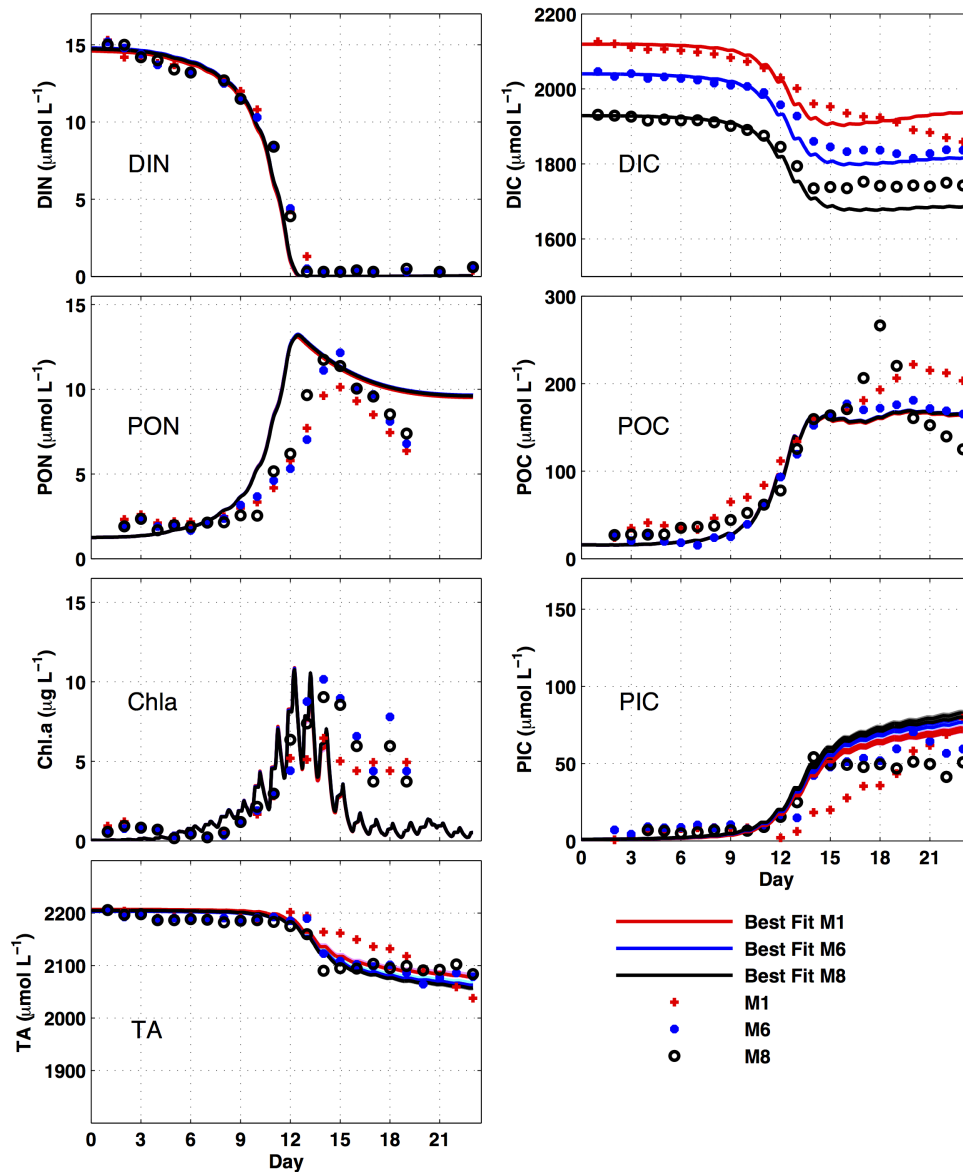
Figure 7. Low calcification solution. The coloured bands represent ensemble of model results according to *a posteriori* and symbols show observations.
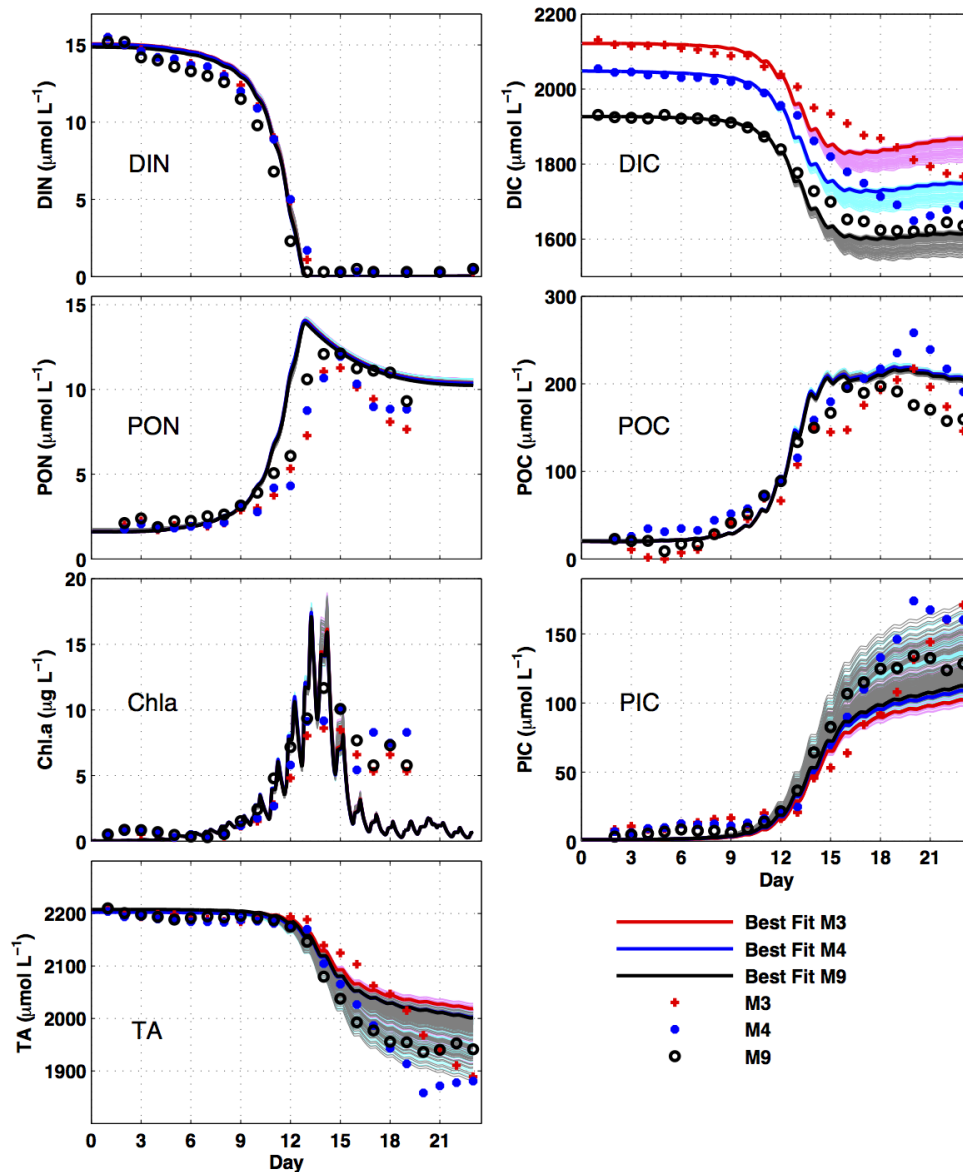
Figure 8. High calcification solution. The coloured bands represent ensemble of model results according to *a posteriori* and symbols show observations.
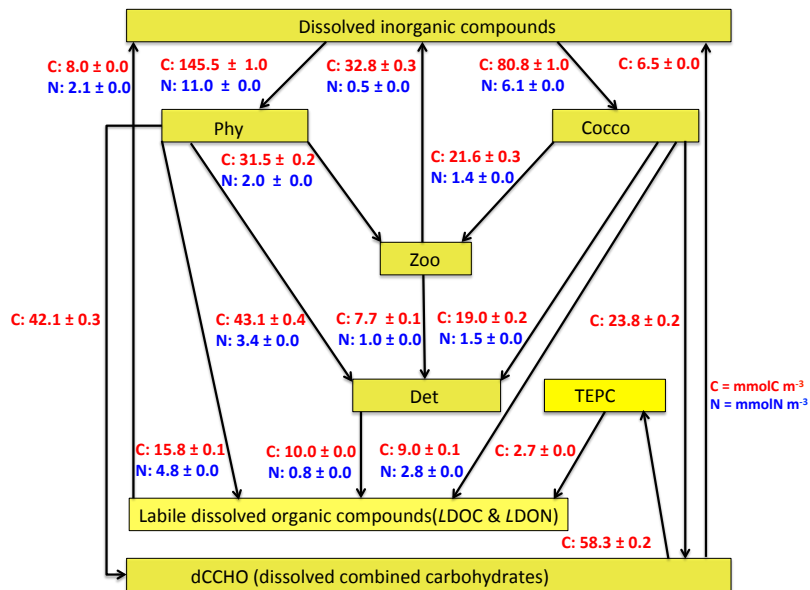
(a) High CO$_2$
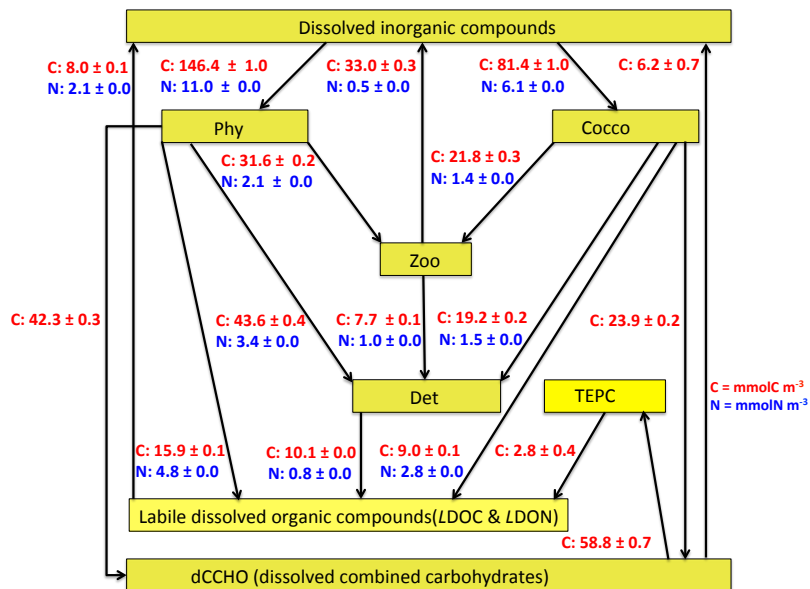
(b) Low CO$_2$

Figure 9. Carbon and nitrogen fluxes estimated by the model in mesocosms with low observed calcification but different CO$_2$ treatment, high (a) and low (b). All the arrows that point downwards show flux estimates from the respective compartment on the right hand side, whereas arrows pointing upwards show values on the left hand side.
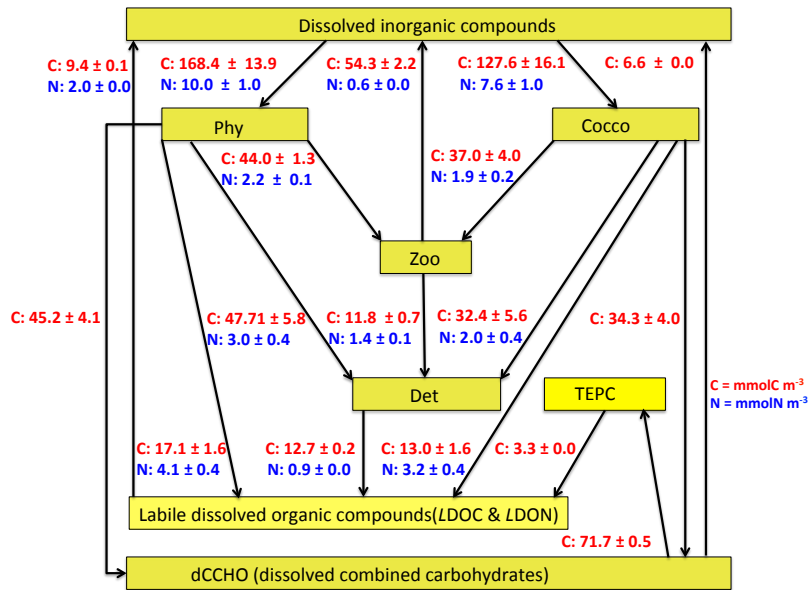
(a) High CO₂
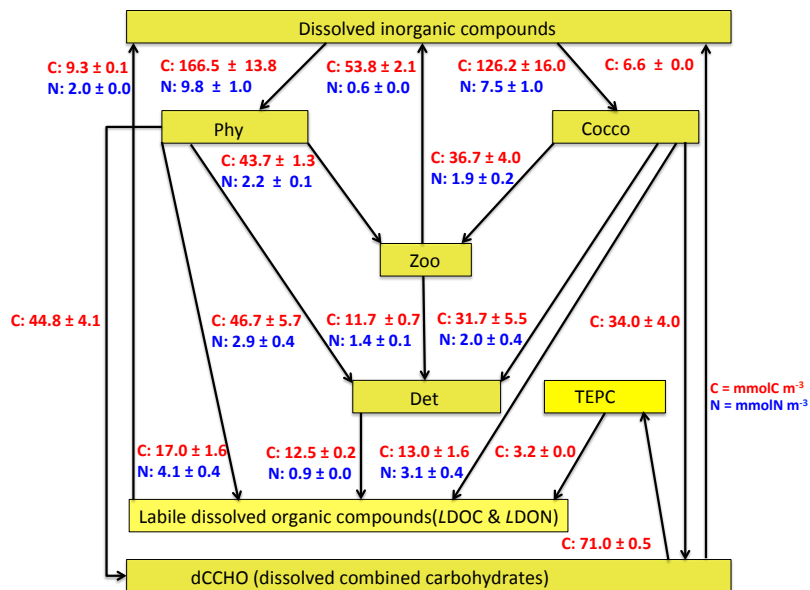
(b) Low CO₂

Figure 10. Carbon and nitrogen fluxes estimated by the model in mesocosms with high observed calcification but different CO_2 treatment, high (a) and low (b). All the arrows that point downwards show flux estimates from the respective compartment on the right hand side, whereas arrows pointing upwards show values on the left hand side.
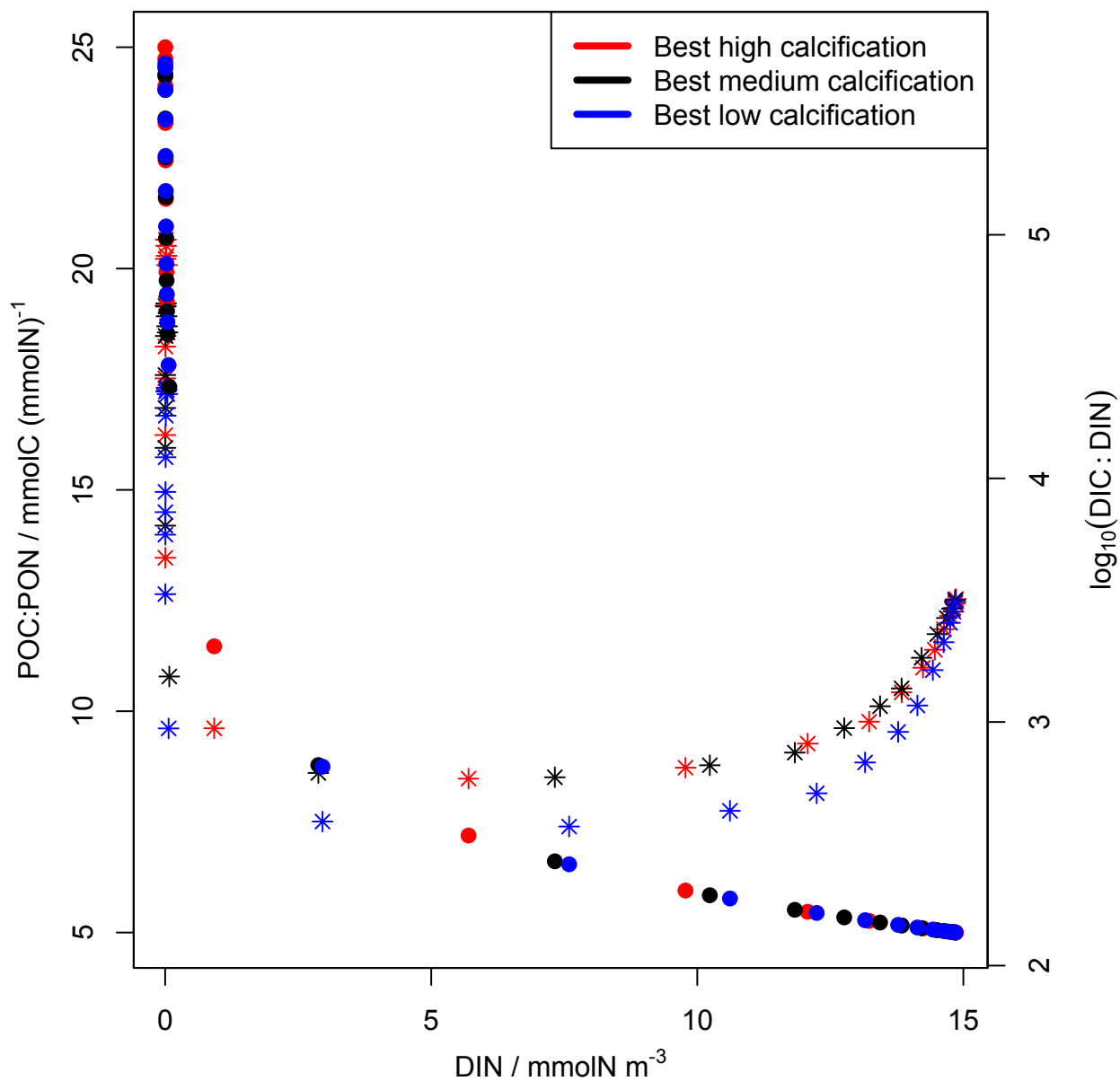
Figure 11. Ratios of [POC]:[PON] and [DIC]:[DIN] determined from daily sampled noon values of model results. Filled circles represent log_{10} (DIC:DIN) ratios. Asteris symbols represent POC:PON ratio over the duration of the experiment.
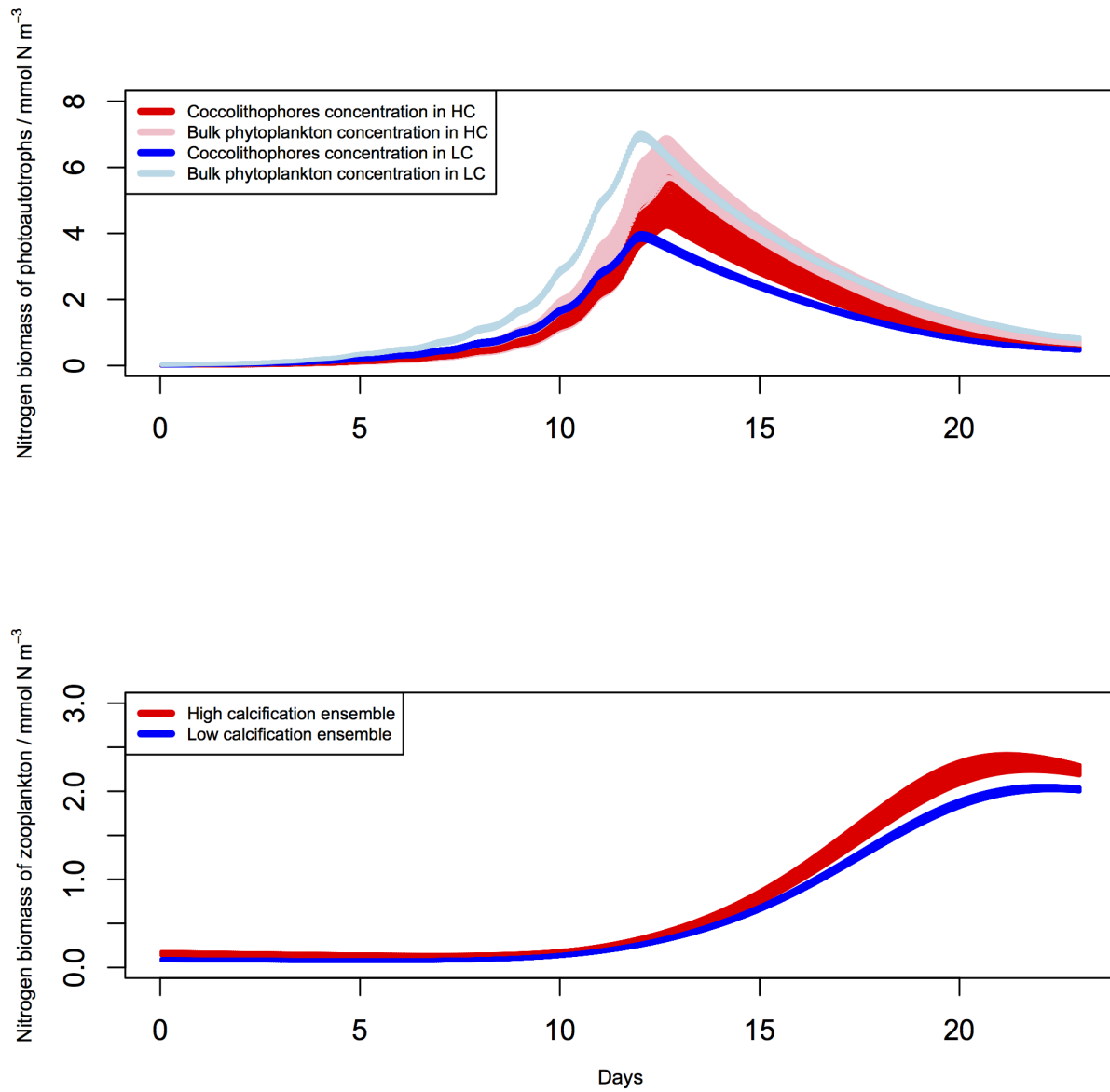
Figure 12. Simulated nitrogen biomass concentrations of photoautotrophs and zooplankton in high and low calcification solutions.
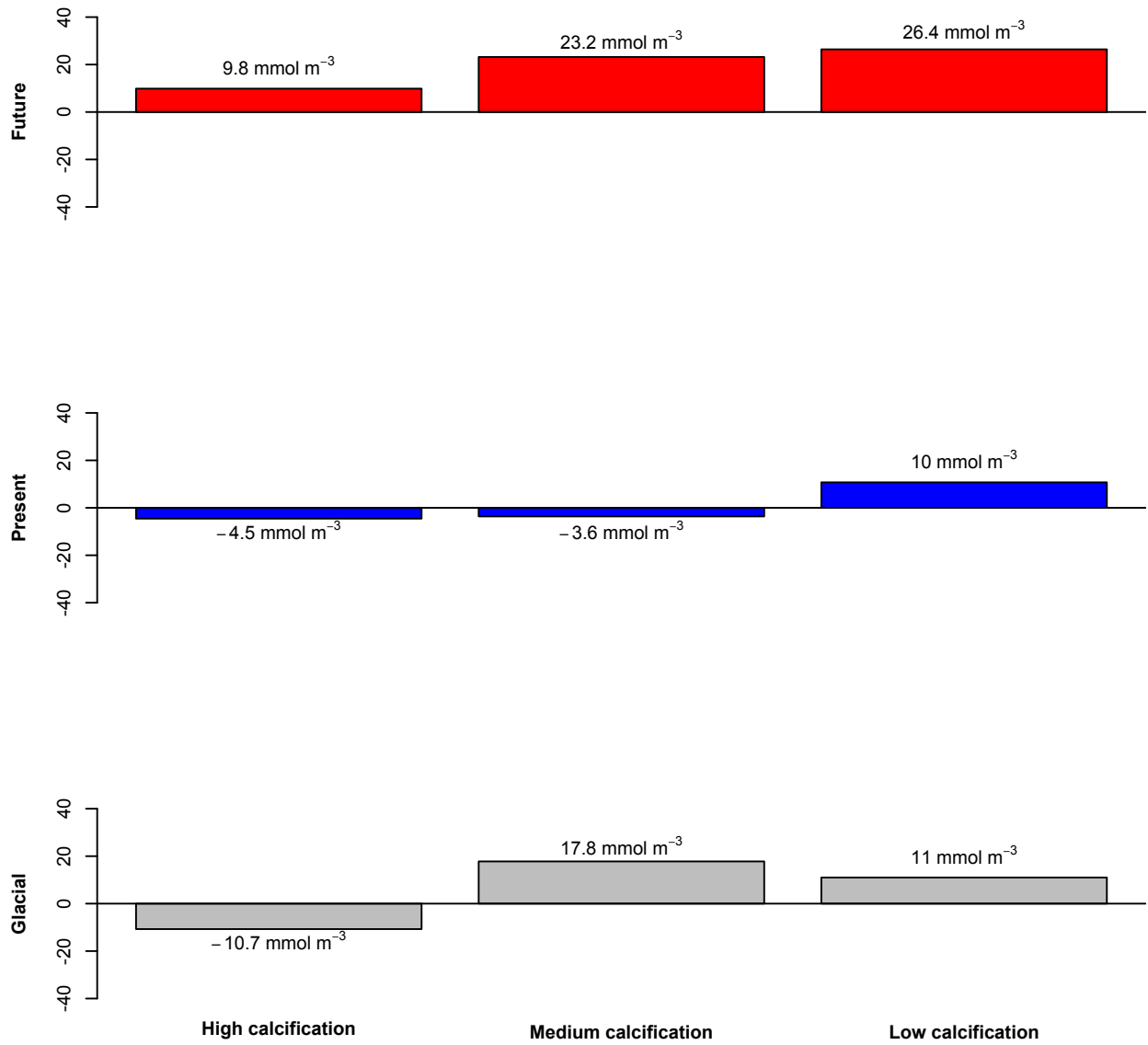
Figure 13. Bar plots depicting cumulative sum of PIC residual (modal-data misfit) from day 13 to day 18 of the experiment for three replicates in mean solution of HC, MC and LC ensembles. First row shows mesocosms with high CO_2 treatment (future), second row medium CO_2 treatment (present) and third row low CO_2 treatment (glacial).
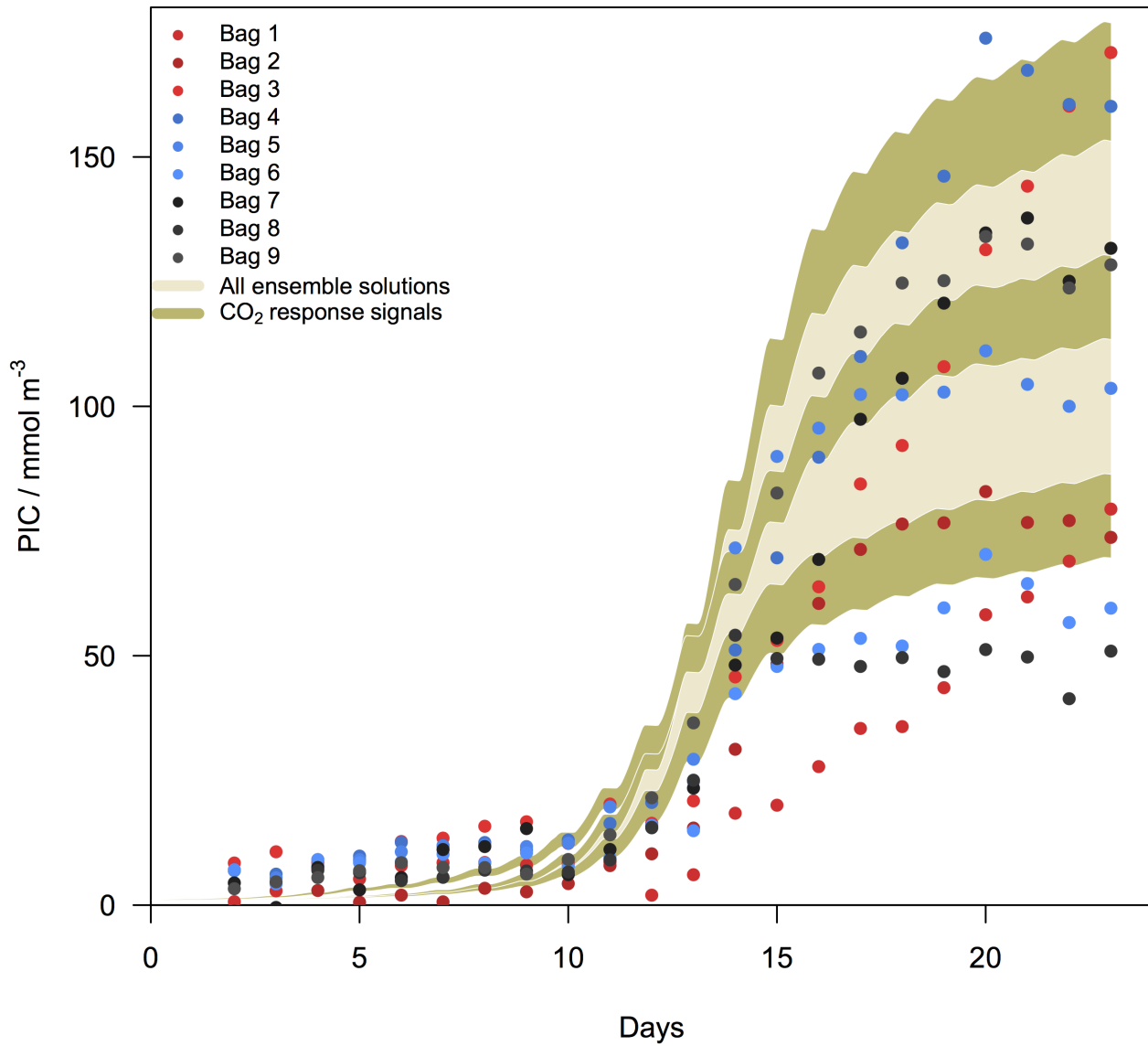
Figure 14. Full spread of model solutions according to credible range in parameter estimates, inlcuding ensemble solutions of high, medium and low calcification (light brown shaded area). Symbols represent observations of all mesocosms. Khaki shaded bands show CO_2 effect in the model, for solutions with lowest, medium and highest calcification rates.

7 Tables

Initial conditions & parameters for optimisation	Description	Unit
1) PON_0	Initial concentration of particulate organic nitrogen	mmol N m^{-3}
2) f_{det}	fraction of PON_0 assigned to non-living detritus	-
3) f_{zoo}	fraction of living PON_0 assigned to zooplankton	-
4) f_{cocco}	Initial coccolithophore fraction of photoautotrophs	-
5) Q_0	subsistence quota (minimum cellular N:C ratio)	mol mol^{-1}
6) α_{cocco}	Photosynthetic efficiency of coccolithophores	mol C (g Chl$a$)$^{-1}$ m^2 W^{-1} d^{-1}
7) α_{phy}	Photosynthetic efficiency of non-calcifying phytoplankton	mol C (g Chl$a$)$^{-1}$ m^2 W^{-1} d^{-1}

Table 1. Initial conditions and model parameters that are subject to optimisation.

Parameter	Description	LC	MC	HC	Units
PON_0	Parameter of initial PON concentration	1.25	1.90	1.61	mmol N m^{-3}
f_{det}	Parameter of initial detritus fraction	0.89	0.89	0.89	-
f_{zoo}	Parameter of initial zoopl. fraction	0.72	0.63	0.88	-
f_{cocco}	Parameter of initial coccolithophore fraction	0.39	0.88	0.40	-
Q_0	Subsistence N:C ratio	$5.5 \cdot 10^{-2}$	$4.2 \cdot 10^{-2}$	$4.2 \cdot 10^{-2}$	-
α_{cocco}	Photosynth. light absorpt. coeff. of coccolithoph.	1.40	0.50	1.66	mol C (g Chl a)$^{-1}$ m^2 W^{-1} d^{-1}
α_{phy}	Photosynth. light absorpt. coeff. of non-calcifiers	1.73	3.10	1.71	mol C (g Chl a)$^{-1}$ m^2 W^{-1} d^{-1}

Table 2. Maximum likelihood parameter estimates of three model solutions: low, medium, and high calcification (LC, MC, and HC)

	f_{det}	f_{zoo}	f_{cocco}	Q_0	α_{cocco}	α_{phy}
PON_0	-0.03 / 0.03 / -0.30	0.57 / 0.48 / 0.51	-0.10 / 0.29 / **0.66**	0.05 / -0.20 / -0.34	0.11 / 0.03 / -0.56	-0.10 / 0.19 / **0.60**
f_{det}	1	-0.51 / -0.33 / **-0.92**	0.13 / 0.01 / -0.28	0.23 / 0.25 / 0.11	-0.15 / -0.10 / 0.10	0.13 / 0.03 / -0.40
f_{zoo}	.	1	-0.47 / 0.24 / 0.5	-0.11 / -0.30 / -0.16	0.50 / 0.52 / -0.38	-0.42 / 0.22 / **0.63**
f_{cocco}	.	.	1	0.10 / -0.12 / -0.25	**-0.99** / -0.15 / **-0.95**	**0.99 / 0.93 / 0.93**
Q_0	.	.	.	1	-0.10 / -0.25 / 0.18	0.13 / 0.10 / -0.26
α_{cocco}	.	.	.	.	1	**-0.97** / -0.18 / **-0.87**
α_{phy}	.	.	.	.	.	1

Table 3. Correlation coefficients of parameter estimates of low, medium, and high calcification model solutions (LC, MC, and HC). Correlation coefficients ≥ 0.6 are marked bold face.

State variable name	LC / mmol N m^{-3}	MC	HC
PON_0	1.2 ± 0.01	1.9 ± 0.01	1.7 ± 0.1
DetN$_0$	$1.1 \pm 4 \cdot 10^{-4}$	$1.7 \pm 1 \cdot 10^{-3}$	1.6 ± 0.01
ZooN$_0$	$0.1 \pm 1 \cdot 10^{-3}$	$0.1 \pm 1 \cdot 10^{-3}$	0.2 ± 0.01
CoccoN$_0$	$0.02 \pm 2 \cdot 10^{-3}$	$0.06 \pm 1 \cdot 10^{-3}$	$0.01 \pm 2 \cdot 10^{-3}$
PhyN$_0$	$0.02 \pm 2 \cdot 10^{-3}$	$0.01 \pm 4 \cdot 10^{-4}$	$0.01 \pm 3 \cdot 10^{-3}$

Table 4. Mean initial values of PON (PON_0), detritus (DetN$_0$), zooplankton (ZooN$_0$), coccolithophores (CoccoN$_0$) and bulk phytoplankton (PhyN$_0$) according to posterior of the (initial condition) parameter estimates of three solutions: low, medium, and high calcification (LC, MC, and HC).

Appendices

A Supplementary model equations

A.1 Arrhenius relation

The affect of temperature on the metabolic rates and biological activities of the vast majority of organisms is given by the Arrhenius relationship (Sibly et al., 2012).

$$T_f = \exp[-A_E.(\frac{1}{T} - \frac{1}{T_{\text{ref}}})] \tag{A.1}$$

where T_{ref} is reference temperature, given in units Kelvin (K). and approximately equals to 293.15 K (Table A.1).

A.2 Photoautotrophs

The resource allocation depends on the cellular nitrogen-to-carbon (N:C) ratio, expressed by the cell quota (Q^N). Q^N is the cellular N biomass normalised to carbon/energy units. The availability of resources that can be allocated is estimated by the relative difference between Q^N from and a subsistence quota (Q_0). Q_0 is the minimum N:C ratio required for a photoautotrophic cell to survive. As Q^N approaches Q_0 less resources can be allocated (e.g. to the light harvesting complex) and algal growth becomes limited. Under balanced optimal conditions we can approximate $f_V \approx f_V^0$ for photoautotrophs. An optimal allocation of nutrients to specific cellular sites (or cell compartments) is thus determined by a trade-off between three fractions: a) a fraction that is allocated to the nutrient acquisition complex (f_V), b) a fraction attached to structural proteins (expressed as Q_s/Q^N), and c) a remaining fraction (1 - f_V - Q_s/Q) that can be allocated to the light harvesting complex and thus promotes the synthesis of chlorophyll *a* (Pahlow et al., 2013). An optimal allocation factor (f_V^0) for nutrient uptake is derived by maximising net growth rate with respect to nutrient uptake and thus f_V (Eq. A.3 in Appendix A). Under nutrient depleted conditions, some higher growth rate of a algal cell can be maintained by increasing f_V^0 to the cost of resources that can be assigned to the light-harvesting complex (referred to as f_{LHC}^0; the optimal allocation factor for LHC). In consequence, the mobilisation of resources (N in this study) for nutrient acquisition (induced by an increase of f_V^0) reduces the rate of chlorophyll *a* synthesis. Vice-versa for light-limited conditions, growth rate of a cell is optimised by investing more resources to light harvesting complex of a cell, which enhances the rate of chlorophyll *a* synthesis. This is achieved for low values of f_V^0.

In the model the optimal allocation factor for light harvesting complex in an algal cell is calculated from f_V^0 and Q_0:

$$Q_s = \frac{Q_0}{2} \tag{A.2}$$

$$f_{V_{phy/cocco}}^0 = \frac{Q_s}{Q_{cocco/phy}^N} - \zeta^N \cdot (Q_{cocco/phy}^N - Q_0) \tag{A.3}$$

$$f^0_{\text{LHC}_{cocco/phy}} = 1 - \frac{Q_s}{Q^N_{cocco/phy}} - f^0_{V_{cocco/phy}} \tag{A.4}$$

where ζ^N is the cost of N uptake in a photoautotrophic cell, given in units mol mol^{-1}; and Q_s is the N quota attached with structural proteins, given in units mol N (mol C)$^{-1}$. In our model maximum N assimilation rate and maximum carbon fixation rates are numerically identical.

$$V^N_{max} = V^N_0 \cdot T_f \tag{A.5}$$

$$V^C_{max} = V^C_0 \cdot T_f \tag{A.6}$$

where V^N_{max} and V^C_{max} are maximum N assimilation and maximum carbon fixation rates, given in units mol N (mol C)$^{-1}$ d^{-1} and mol C (mol C)$^{-1}$ d^{-1}. Model parameters V^N_0 and V^C_0 are photoautotrophic potential N assimilation and C fixation rates, given in units mol N (mol C)$^{-1}$ d^{-1} and mol C (mol C)$^{-1}$ d^{-1}(Table A.1).

The total N uptake rate of photoautotrophs is calculated from the local N uptake rate (Pahlow et al., 2013). The latter is calculated from maximum N assimilation rate, potential nutrient affinity and dissolved inorganic nitrogen concentration (DIN).

$$\hat{V}^N = \left(\sqrt{\frac{1}{V^N_{max}}} + \sqrt{\frac{1}{A_0 \cdot (\text{DIN})}}\right)^{-2} \tag{A.7}$$

$$V^N_{phy/cocco} = f^0_{V_{cocco/phy}} \cdot \hat{V}^N \tag{A.8}$$

where $\hat{V}^N$ is the local N uptake of photoautotrophs, given in units mol N (mol C)$^{-1}$ d^{-1}. A_0 is potential nutrient affinity of respective algae in units m^3 (mol C)$^{-1}$ d^{-1} (Table A.1).

The gross carbon fixation rate of calcifiers and non-calcifiers is calculated from day length, degree of light saturation, f^0_{LHC} and V^C_{max}:

$$V^C_{cocco/phy} = L_d \cdot f0^{\text{LHC}}_{cocco/phy} \cdot V^C_{max} \cdot S^{cocco/phy}_I \tag{A.9}$$

where $V^C_{cocco/phy}$ is the gross carbon-fixation by photoautotrophs, given in units mol C (mol C)$^{-1}$ d^{-1}, L_d is the day length as a fraction of 24 hours. For more details see Table (A.1). $S^{phy/cocco}_I$ is the degree of light saturation in photoautotrophs and calculated as:

$$S^{cocco/phy}_I = 1 - \exp\left(-\frac{\alpha \cdot \hat{\theta}_{cocco/phy} \cdot I}{V^C_0}\right) \tag{A.10}$$

$\hat{\theta}_{cocco/phy}$ is Chl:C ratio in the chloroplast of a cell (Pahlow and Oschlies, 2009; Pahlow et al., 2013), given in units mg Chl (mmol C)$^{-1}$.

The differential equations of C and N biomass for phytoplankton and coccolithophores are:

$$\frac{d}{dt}\text{PhyC} = (\mu_{phy} - CN_{fact} \cdot \gamma_N) \cdot \text{PhyC} - \frac{A_{phy}}{Q_{phy}^N} - \frac{G_{phy}}{Q_{phy}^N} \tag{A.11}$$

$$\frac{d}{dt}\text{CoccoC} = (\mu_{cocco} - CN_{fact} \cdot \gamma_N) \cdot \text{CoccoC} - \frac{A_{cocco}}{Q_{cocco}^N} - \frac{G_{cocco}}{Q_{cocco}^N} \tag{A.12}$$

$$\frac{d}{dt}\text{PhyN} = V_{phy}^N \cdot \text{PhyC} - \gamma_N \cdot \text{PhyN} - A_{phy} - G_{phy} \tag{A.13}$$

$$\frac{d}{dt}\text{CoccoN} = V_{cocco}^N \cdot \text{CoccoC} - \gamma_N \cdot \text{CoccoN} - A_{cocco} - G_{cocco} \tag{A.14}$$

A description of auxiliary variables is given in Table (A.1). We stress that the parameterisations in Eqs. (A.11 and A.12) are identical for both photoautrophic groups (coccolithophores and non-calcifying algae), but some of the corresponding optimised parameter values may turn out to be different between the two.

The differential equations for chlorophyll a of non-calcifying phytoplankton (with subscripts phy) and coccolithophores ($cocco$) are:

$$\frac{d}{dt}\text{Chl}_{cocco/phy} = (\mu_{cocco/phy} + \frac{\dot{\theta}_{cocco/phy}}{\theta_{cocco/phy}}) \cdot \text{Chl}_{cocco/phy} - A_{cocco/phy} \cdot \theta_{cocco/phy}^N - G_{cocco/phy} \cdot \theta_{cocco/phy}^N \tag{A.15}$$

Where $\theta_{cocco/phy}^N$ are the respective cellular Chl:N ratios in units mg Chl (mmol N)$^{-1}$ (Table A.1). The terms $\dot{\theta}_{cocco/phy}$ are the time derivatives of $\theta_{cocco/phy}$. The regulation of θ_{phy} and θ_{cocco} upon on the buildup and limitation of chlorophyll a is determined by optimality-based criteria.

The regulation term for chlorophyll a synthesis (S_{chl}) is given as:

$$S_{chl} = \frac{\dot{\theta}_{cocco/phy}}{\theta_{cocco/phy}} = (\frac{1}{\zeta^{Chl}} \cdot \frac{\partial A_{cocco/phy}}{\partial \hat{\theta}_{cocco/phy}}) + \dot{Q}_{cocco/phy}^N \cdot \frac{\hat{\theta}_{cocco/phy}}{\theta_{cocco/phy}} \cdot (\frac{2 \cdot Q_s}{Q_{cocco/phy}^N \cdot Q_{cocco/phy}^N} + \zeta^N) \tag{A.16}$$

$$\frac{\partial A_{cocco/phy}}{\partial \hat{\theta}_{cocco/phy}} = L_d \cdot V_{max}^C \cdot [\frac{\alpha_{cocco/phy} \cdot I}{V_{max}^C} \cdot (1 - S_I^{cocco/phy}) \cdot (1 - \zeta^{Chl} \cdot \hat{\theta}_{cocco/phy}) - S_I^{cocco/phy} \cdot \zeta^{Chl}] - R_M^{Chl} \cdot \zeta^{Chl} \tag{A.17}$$

where, A is an auxiliary variable that contains all light dependent terms (Pahlow and Oschlies, 2009; Pahlow et al., 2013) and has the unit d^{-1}; ζ^{Chl} and ζ^N are costs of chlorophyll a synthesis and N assimilation, given in units mol C (g Chl)$^{-1}$ and mol C (mol N)$^{-1}$ (Table A.1). The derivative term ($\frac{\partial A}{\partial \hat{\theta}}$) is given in units mol C (g Chl)$^{-1}$ d^{-1}.

A.3 Respiration costs

Total respiration cost in a cell includes costs due to chlorophyll synthesis, nutrient acquisition and cell maintenance.

$$r_{phy/cocco}^c = R_{phy/cocco}^{Chl} + \zeta^N \cdot V_{phy/cocco}^N + R_M \tag{A.18}$$

where respiration cost due to synthesis of chlorophyll a is given as:

$$R_{phy/cocco}^{Chl} = (V_{phy}^C + f0_{phy/cocco}^{\text{LHC}} \cdot R_M^{Chl}) \cdot \zeta^{Chl} \cdot \hat{\theta}_{phy/cocco} \tag{A.19}$$

where R_M is maintenance respiration cost of a cell, given in units d^{-1}. Detailed description of auxiliary variables is given in the Table (A.1).

A.4 PIC formation and regulation of calcification

PIC formation can be written as a single differential equation:

$$\frac{d}{dt}\text{PIC} = (f_{\text{CO}_2} \cdot f_{\text{PIC}} \cdot \mu_{cocco}) \cdot \text{CoccoC} - \tau_{dissol} \cdot \text{PIC} \tag{A.20}$$

where τ_{dissol} is the dissolution rate of PIC, given in units d^{-1}. Parameterisation of calcite-to-C_{organic} ratio is given by Eq. (A.21), whereas regression model of Findlay et al. (2011) to quantify effect of different CO_2 concentrations on PIC formation is represented by Eq. (A.22).

$$f_{\text{PIC}} = \frac{1}{2} + \frac{s_{\text{PIC}}}{1 + \exp(s_{\text{PIC}} \cdot f0_{cocco}^{\text{LHC}})} \tag{A.21}$$

$$f_{\text{CO}_2} = -0.0097 \cdot \text{CO}_{2\,aq} + 0.9654 \tag{A.22}$$

with aqueous carbon dioxide $CO_{2\,aq}$ concentrations normalised to water mass instead of volume, given in units μmol kg^{-1}. A reference rate of PIC formation under nutrient replete and light saturated conditions is prescribed as a molar ratio of $f_{\text{PIC}} = 0.5$ mol PIC formed per mol C assimilated into organic matter, Eq. (A.21). The molar ratio (f_{PIC}) is assumed to increase when the fraction of resources allocated to the light harvesting complex (LHC) of a cell ($f0_{cocco}^{\text{LHC}}$) decreases. According to our model approach the process of calcification can be interpreted as an additional pathway for dissipating excess energy (Barcelos e Ramos et al., 2012), as is the case under high light conditions when chlorophyll a synthesis rates diminish (induced by a reduction of $f0_{cocco}^{\text{LHC}}$). On the one hand, PIC formation becomes enhanced under high light conditions, while less resources become allocated to light harvesting complex. On the other hand, calcification is reduced or ceases under conditions of low or no light. Under nutrient depleted conditions, when more resources become allocated to nutrient uptake sites rather than to light harvesting complex, the rate of calcification per net carbon fixation also increases. For low (nutrient limited) growth rates under saturated (or high) light conditions the parameterisation f_{PIC} can yield maxima in the calcite-to-C_{organic} ratio (of the calcifying algae) that may reach values of 2 and slightly above. The function f_{CO_2} in Eq. (A.20) has no dimension and it simulates the effect of varying CO_2 concentrations on f_{PIC}.

A.5 Zooplankton

The sms differential equations for zooplankton carbon and nitrogen biomass are:

$$\frac{d}{dt}\text{ZooC} = \frac{G_{phy}}{Q_{phy}^N} + \frac{G_{cocco}}{Q_{cocco}^N} - r_{zoo} - \frac{M_{zoo}}{Q_{zoo}} \tag{A.23}$$

$$\frac{d}{dt}\text{ZooN} = G_{phy} + G_{cocco} - \gamma_{zoo}^{N} - M_{zoo} \tag{A.24}$$

Equations below represent Holling type III grazing dynamics.

$$G_{phy} = g_m \cdot \frac{(\text{PhyN}^2)}{\epsilon + (\text{PhyN}^2)} \cdot \text{ZooN} \tag{A.25}$$

$$G_{cocco} = g_m \cdot \frac{(\text{CoccoN}^2)}{\epsilon + (\text{CoccoN}^2)} \cdot \text{ZooN} \tag{A.26}$$

where g_m is the nitrogen specific maximum grazing rate on photoautotrophs, given in units d^{-1}; and ϵ is the half saturation constant for grazing, given in units $(\text{mmol N})^2 \, m^{-6}$.

A.6 Zooplankton respiration and excretion

Respiration is parameterized as a function of respiration maintenance rate coefficient, temperature dependent metabolic rates and carbon concentration of heterotroph.

$$r_{zoo} = R_{basal} \cdot T_f \cdot \text{ZooC} \tag{A.27}$$

Similarly, excretion is parameterised as a function of respiration maintenance rate to basal metabolism, temperature dependent metabolic rates and nitrogen concentration of heterotroph.

$$\gamma_{zoo} = R_{basal} \cdot T_f \cdot \text{ZooN} \tag{A.28}$$

A.7 Detritus

The corresponding differential equations of detrital C and N mass are:

$$\frac{d}{dt}\text{DetC} = \frac{A_{phy}}{Q_{phy}^N} + \frac{A_{cocco}}{Q_{cocco}^N} + \frac{M_{zoo}}{Q_{zoo}} - \omega_{det} \cdot T_f \cdot \text{DetC} \tag{A.29}$$

$$\frac{d}{dt}\text{DetN} = A_{phy} + A_{cocco} + M_{zoo} - \omega_{det} \cdot T_f \cdot \text{DetN} \tag{A.30}$$

Aggregation equations for bulk phytoplankton and coccolithophores are given below.

$$A_{phy} = \phi_{agg} \cdot \text{PhyN} \cdot \text{DetN} + \phi_{agg} \cdot \text{PhyN}^2 \tag{A.31}$$

$$A_{cocco} = \phi_{agg} \cdot \text{CoccoN} \cdot \text{DetN} + \phi_{agg} \cdot \text{CoccoN}^2 \tag{A.32}$$

A.8 Dissolved inorganic compounds (DIN, DIC) and total alkalinity (TA)

The nitrogen uptake ($V_{cocco/phy}^{N}$) is carbon-specific and is therefore given as a rate of N utilisation per carbon, in units mol N (mol C)$^{-1}$ d^{-1} (Pahlow and Oschlies, 2009):

$$\frac{d}{dt}\text{DIN} = -(V_{phy}^{N} \cdot \text{PhyC} + V_{cocco}^{N} \cdot \text{CoccoC}) + \gamma_{zoo}^{N} + \rho \cdot T_f \cdot LDON \tag{A.33}$$

The sources of DIN are calculated from zooplankton excretion (γ_{zoo}^{N}) and the remineralisation of $LDON$.

The sms differential equation for DIC is given below:

$$\frac{d}{dt}\text{DIC} = -\mu_{phy} \cdot \text{PhyC} - (1 + f_{CO_2} \cdot f_{pic}) \cdot \mu_{cocco} \cdot \text{CoccoC} + \tau_{dissol} \cdot \text{PIC} + r_{zoo} + \rho \cdot T_f \cdot (LDOC + \text{dCCHO}) + \text{F}_{\text{DIC}} \tag{A.34}$$

Calculations of air-sea gas exchange (F$_{\text{DIC}}$) within mesocosms are based on original carbonate chemistry code provided by the Ocean Carbon-Cycle Model Intercomparison Project (Orr, 1999). The original code was refined to include an accelerated iteration scheme for pH and pCO$_2$ calculations (Christoph Völker, personal communication), as already applied in Schartau et al. (2007).

The differential equation listed below accounts for TA in the system:

$$\frac{d}{dt}\text{TA} = (1 + 1/16) \cdot \left(\frac{V_{phy}^{N}}{Q_{phy}^{N}} \cdot \text{PhyN} + \frac{V_{cocco}^{N}}{Q_{cocco}^{N}} \cdot \text{CoccoN}\right) - 2 \cdot (f_{CO_2} \cdot f_{PIC} \cdot \mu_{cocco} \cdot \text{CoccoC} - \tau_{dissol} \cdot \text{PIC})$$
$$- (1 + 1/16) \cdot \rho \cdot T_f \cdot LDON \tag{A.35}$$

Measured values of DIN, TA, and DIC on day one of the experiment were taken as initial conditions for respective mesocosms.

A.9 Dissolved labile organic matter

The differential equations for dissolved organic matter are given below:

$$\frac{d}{dt}LDOC = C_{fact} \cdot \gamma_N \cdot \left[(1 - f_{\text{dCCHO}}^{phy}) \cdot \text{PhyC} + (1 - f_{\text{dCCHO}}^{cocco}) \cdot \text{CoccoC}\right] + \omega_{det} \cdot T_f \cdot \text{DetC}$$
$$+ \omega_{gel} \cdot T_f \cdot \text{TEPC} - \rho \cdot T_f \cdot LDOC \tag{A.36}$$

$$\frac{d}{dt}LDON = \gamma_N \cdot (\text{PhyN} + \text{CoccoN}) + \omega_{det} \cdot T_f \cdot \text{DetN} - \rho \cdot T_f \cdot LDON \tag{A.37}$$

A.10 dCCHO and TEPC

The differential equation for dissolved combined carbohydrates(dCCHO) is given as:

$$\frac{d}{dt}\text{dCCHO} = C_{fact} \cdot \gamma_N \cdot \left[f_{\text{dCCHO}}^{phy} \cdot \text{PhyC} + f_{\text{dCCHO}}^{cocco} \cdot \text{CoccoC}\right] - \phi_{\text{dCCHO}} \cdot \text{dCCHO}^2 - \phi_{\text{TEP}} \cdot \text{dCCHO} \cdot \text{TEPC}$$
$$- \rho \cdot T_f \cdot \text{dCCHO} \tag{A.38}$$

Given below is the parameterisation to estimate the fraction of phytoplankton exudates that become available to be part of dCCHO during two distinct modes of carbon overconsumption decscribed in Schartau et al. (2007).

$$f_{\text{dCCHO}}^{cocco/phy} = \left[1 + p_{\text{dCCHO}} \cdot \exp(1 - Q_s/Q_{cocco/phy}^N)\right]^{-1} \tag{A.39}$$

where p_{dCCHO} is the fraction of DOC that enters dCCHO pool. Coagulation parameter of dCCHO (ϕ_{dCCHO}) is derieved from product of α_{dCCHO} (stickiness between dCCHO and dCCHO) and β_{dCCHO} (C-specific collision rates between dCCHO and dCCHO). Likewise, coagulation parameter of dCCHO-TEPC (ϕ_{TEPC}) is computed from the product of α_{TEPC} (stickiness between dCCHO and TEPC) and β_{TEPC} (C-specific collision rates between dCCHO and TEPC). α_{dCCHO} and α_{TEPC} have no units as they are probabilities, whereas β_{dCCHO} and β_{TEPC} are given in units m^3 (mmol C)$^{-1}$ d^{-1}. Values of α_{dCCHO} , α_{TEPC} , β_{dCCHO} and β_{TEPC} are taken from (Schartau et al., 2007).

$$\begin{aligned}
\phi_{\text{dCCHO}} &= \alpha_{\text{dCCHO}} \cdot \beta_{\text{dCCHO}} \\
\phi_{\text{dCCHO}} &= (0.87 \cdot 10^{-3}) \cdot 0.86 = 7.48 \cdot 10^{-4}
\end{aligned} \tag{A.40}$$

$$\begin{aligned}
\phi_{\text{TEPC}} &= \alpha_{\text{TEPC}} \cdot \beta_{\text{TEPC}} \\
\phi_{\text{TEPC}} &= 0.4 \cdot 0.064 = 2.56 \cdot 10^{-2}
\end{aligned} \tag{A.41}$$

The differential equation for formation of TEPC is shown below:

$$\frac{d}{dt}\text{TEPC} = \phi_{\text{dCCHO}} \cdot \text{dCCHO}^2 + \phi_{\text{TEP}} \cdot \text{dCCHO} \cdot \text{TEPC} - \omega_{gel} \cdot T_f \cdot \text{TEPC} \tag{A.42}$$

Auxiliary variables & functions	Description	Unit
T_f	Arrhenius temperature dependency	-
f_V	resource fraction allocated for nutrient acquisition	-
f_V^0	optimal allocation value of f_V	-
f_{LHC}^0	optimal resource allocation to light harvesting complex (LHC)	-
μ	net growth rates of respective photoautotrophs	d^{-1}
Q_s	N quota attached with structural proteins	mol N (mol C)$^{-1}$
$\hat{V}^N$	photoautotrophic local N uptake rate of rate	mol N (mol C)$^{-1}$ d^{-1}
V^C	photoautotophic gross carbon fixation rates	mol C (mol C)$^{-1}$ d^{-1}
r^C	respiration rates	d^{-1}
V_{max}^N	photoautotrophic maximum N assimilation rates	mol N (mol C)$^{-1}$ d^{-1}
V_{max}^C	photoautotrophic maximum C fixation rates	mol C (mol C)$^{-1}$ d^{-1}
V^N	carbon-specific nitrogen uptake rate	mol N (mol C)$^{-1}$ d^{-1}
Q^N	molar cellular nitrogen-to-carbon (N:C) ratio (cell quota)	mol N (mol C)$^{-1}$
θ	chlorophyll a-to-carbon (Chl:C) ratio of photoautotrophs	g Chl (mol C)$^{-1}$
$\dot{\theta}$	time derivative of θ	g Chl (mol C)$^{-1}$ d^{-1}
θ^N	chlorophyll a-to-nitrogen (Chl:N) ratio of photoautotrophs	g Chl (mol N)$^{-1}$
S_I	degree of light saturation for photosynthesis	-
S_{chl}	regulation term for chlorophyll synthesis	mol C (mol N)$^{-1}$
L_d	day length as a fraction of 24 hours	-
I	Mean irradiance	Wm^{-2} d^{-1}
$\hat{\theta}$	photoautotrophic chloroplast Chl:C ratio	g Chl (mol C)$^{-1}$
A	variable representing all light-dependent terms	d^{-1}
G	nitrogen-specific rates of zooplankton grazing	mmol N m^{-3} d^{-1}
r_{zoo}	zooplankton respiration	mmol C m^{-3} d^{-1}
γ_{zoo}^N	zooplankton excretion of nitrogen	mmol N m^{-3} d^{-1}
M_{zoo}	nitrogen-specific zooplankton mortality	mmol N m^{-3} d^{-1}
A	nitrogen-specific rates of aggregation	mmol N m^{-3} d^{-1}
f_{PIC}	calcification relative to net carbon fixation	mol PIC (mol C)$^{-1}$
F_{DIC}	flux due to air-sea gas exchange	mmol C m^{-3} d^{-1}
f_{CO2}	regression model of CO_2 effect on calcification	-
f_{dCCHO}	fraction of exudates assigned to dCCHO	-
α_{dCCHO}	stickiness between dCCHO and dCCHO	-
β_{dCCHO}	C-specific collision rates between dCCHO and dCCHO	m^3 (mmol C)$^{-1}$ d^{-1}
α_{TEPC}	stickiness between dCCHO and TEPC	-
β_{TEPC}	C-specific collision rates between dCCHO and TEPC	m^3 (mmol C)$^{-1}$ d^{-1}

Model parameters (fixed)		Value	
1) γ_N	photoautotrophic loss rate of organic nitrogen	0.1	d^{-1}
2) CN_{fact}	enhancement factor of carbon exudation relative to γ_N	1.0	-
3) ρ	remineralisation rate of dissolved organic matter	0.05	d^{-1}
4) ω_{det}	hydrolysis/degradation rate of detritus	0.02	d^{-1}
5) ω_{gel}	hydrolysis/degradation rate of TEPC	0.01	d^{-1}
6) τ_{dissol}	dissolution rate of particulate inorganic carbon	0.01	d^{-1}
7) ϕ_{dCCHO}	coagulation parameter of dCCHO	$7.48 \cdot 10^{-4}$	m^3 (mmol C)$^{-1}$ d^{-1}
8) ϕ_{TEPC}	coagulation parameter of dCCHO-TEPC	$2.56 \cdot 10^{-2}$	m^3 (mmol C)$^{-1}$ d^{-1}
9) T_{ref}	reference temperature for A_E relation	293.15	K
10) A_E	slope of arrhenius relationship	4500	K
11) a_w	light attenuation due to water column	0.04	m^{-1}
12) a_c	light attenuation due to chlorophyll a	0.05	(mg Chl$a$)$^{-1}$ m^3
13) R_M^{Chl}	cost of chlorophyll maintenance	0.1	d^{-1}
14) R_M	total respiration maintenance cost	0.05	d^{-1}
15) ζ^{Chl}	cost of photosynthesis coefficient	0.6	mol C (g Chl$a$)$^{-1}$
16) ζ^N	cost of N uptake	0.7	mol C (mol N)$^{-1}$
17) A_0	potential nutrient affinity	1	m^3 mol C^{-1} d^{-1}
18) V_0^N	photoautotrophic potential N assimilation rate	4.0	mol C (mol N)$^{-1}$
19) V_0^C	photoautotrophic potential C fixation rate	4.0	mol C (mol C)$^{-1}$
20) γ_N	algal nitrogen loss rate	0.1	d^{-1}
21) ϕ_{agg}	aggregation rate	0.01	m^3 (mmol N)$^{-1}$ d^{-1}
22) P_{dCCHO}	minimum DOC fraction allocated to dCCHO	0.2	
23) g_m	nitrogen specific maximum grazing rate	0.2	d^{-1}
24) ϵ	prey capture rate normalised to maximum grazing rate	1	(mmol N)^2 m^{-6}
25) M_{zoo}	mortality rate of zooplankton	0.05	d^{-1}
26) R_{basal}	zooplankton basal respiration rate	0.05	d^{-1}
27) p_{PIC}	slope of ΔPIC formed per ΔC assimilated	5.0	mol PIC (mol C)$^{-1}$

Table A.1. Auxiliary model variables and model parameters.

B Data assimilation

B.1 Parameter optimisation procedure

The entire optimisation procedure of each (LC, MC, and HC) case is subject to five consecutive analysis steps:

1) adjustment of parameters while considering published typical values $\longrightarrow$ specify model solution that is in qualitative (visual) good agreement with observations of the medium calcification MC case

2) application of *simulated annealing* algorithm (SANN), see (Bélisle, 1992), to effectively scan and minimise the seven-dimensional manifold $(\Theta, J(\Theta))$, while avoiding to get trapped into local minima of $J(\Theta) \longrightarrow$ obtain global estimate of Θ

3) local refinement of the parameter estimate, using the *Broyden-Fletcher-Goldfarb-Shanno* (BFGS) algorithm (Broyden, 1970; Fletcher, 1970; Goldfarb, 1970; Shanno, 1970) $\longrightarrow$ identify maximum likelihood estimate that corresponds with the global minimum $(\widehat{\Theta}, , J(\widehat{\Theta}))$

4) calculation of the inverse of second derivatives of $J(\Theta)$ with respect to every parameter ($\mathcal{H}_{jj} = \partial^2 J / \partial \Theta_j^2$ at $\widehat{\Theta}$, which is a point-wise approximation of the diagonal elements of a Hessian matrix $\mathcal{H}$) $\longrightarrow$ derive marginal errors (standard errors, $\sqrt{\mathcal{H}_{jj}^{-1}}$) of the estimated parameter values

5) application of a *Markov Chain Monte Carlo* (MCMC) method, using the marginal error information of 4) to confine credible range of optimal parameter values $\longrightarrow$ derive posterior confidence limits of parameter estimates and collinearities (correlations) between parameter estimates.

For steps 2, 3, and 5 the R package FME is applied, as coded and described by Soetaert and Petzoldt (2010). The plankton ecosystem model was coded and compiled as shared library in FORTRAN so that we can apply a FORTRAN-R wrapper function. This wrapper allows us to take advantage of fast numerical Euler forward integrations of the model equations while, at the same time, we can benefit from the R platform and its freely available packages. The cost function $J(\Theta)$ is evaluated in R. The Markov Chain Monte Carlo (MCMC) method employed here is based on the *Adaptive Metropolis-Hastings* (AMH) algorithm (Haario et al., 2001), which is also available with the R package FME. The AMH algorithm generates a new parameter vector (Θ^*) by perturbing the original vector Θ, inferred from a "proposal" distribution (Metropolis et al., 1953). The standard deviation information required for generating the initial proposal (Gaussian) distribution in the AMH algorithm is derived from the diagonal elements of Hessian matrix. We approximated the diagonal elements of the Hessian with finite central differences, as described in e.g. Matear (1995), Kidston et al. (2011), and in Kreus and Schartau (2015). To do so we imposed an incremental step size of 1% variation to the respective parameter values.

B.2 Data correlation matrices

Correlations during pre-bloom (t_i; i = 1, ... , 13) between mesocosms with medium observed calcification in matrix form are given below:

$$
C_{(\mathbf{y})} =
\begin{pmatrix}
 & \text{DIC} & \text{DIN} & \text{Chl}a & \text{PON} & \text{POC} & \text{PIC} & \text{TA} \\
\text{DIC} & 1 & 0.57 & -0.95 & -0.77 & -0.95 & -0.89 & 0.88 \\
\text{DIN} & . & 1 & -0.56 & -0.52 & -0.53 & -0.58 & 0.53 \\
\text{Chl}a & . & . & 1 & 0.71 & 0.91 & 0.81 & -0.77 \\
\text{PON} & . & . & . & 1 & 0.87 & 0.77 & -0.65 \\
\text{POC} & . & . & . & . & 1 & 0.83 & -0.77 \\
\text{PIC} & . & . & . & . & . & 1 & -0.95 \\
\text{TA} & . & . & . & . & . & . & 1
\end{pmatrix}
\tag{B.1}
$$

5   Correlations during post-bloom period (t_i; i = 14, ... , 22) are:

$$
C_{(\mathbf{y})} =
\begin{pmatrix}
 & \text{DIC} & \text{DIN} & \text{Chl}a & \text{PON} & \text{POC} & \text{PIC} & \text{TA} \\
\text{DIC} & 1 & 0.22 & 0.27 & 0.29 & -0.83 & -0.93 & 0.94 \\
\text{DIN} & . & 1 & 0.3 & 0.31 & -0.23 & -0.22 & 0.24 \\
\text{Chl}a & . & . & 1 & 0.99 & 0.01 & -0.44 & 0.49 \\
\text{PON} & . & . & . & 1 & -0.02 & -0.45 & 0.50 \\
\text{POC} & . & . & . & . & 1 & 0.65 & -0.64 \\
\text{PIC} & . & . & . & . & . & 1 & -0.99 \\
\text{TA} & . & . & . & . & . & . & 1
\end{pmatrix}
\tag{B.2}
$$

Residual standard errors (σ_i) were calculated based on daily measurements between the mesocosms of similar observed calcification and can be written in matrix notation with off-diagonal elements being zero:

$$
S_i =
\begin{pmatrix}
\sigma_i^{(\text{DIC})} & 0 & \cdots & 0 \\
0 & \sigma_i^{(\text{DIN})} & \cdots & \vdots \\
\vdots & \vdots & \ddots & 0 \\
0 & \cdots & 0 & \sigma_i^{(\text{TA})}
\end{pmatrix}
\tag{B.3}
$$

References

Arteaga, L., Pahlow, M., and Oschlies, A. (2014). Global patterns of phytoplankton nutrient and light colimitation inferred from an optimality-based model. *Global Biogeochemical Cycles*, 28(7):648–661.

Barcelos e Ramos, J., Müller, M., and Riebesell, U. (2010). Short-term response of the coccolithophore *Emiliania huxleyi* to an abrupt change in seawater carbon dioxide concentrations. *Biogeosciences*, 7(1):177–186.

Barcelos e Ramos, J., Schulz, K. G., Febiri, S., and Riebesell, U. (2012). Photoacclimation to abrupt changes in light intensity by *Phaeodactylum tricornutum* and *Emiliania huxleyi*: the role of calcification. *Marine Ecology Progress Series*, 452:11–26.

Bélisle, C. J. (1992). Convergence theorems for a class of simulated annealing algorithms on rd. *Journal of Applied Probability*, pages 885–895.

Broyden, C. G. (1970). The convergence of a class of double-rank minimization algorithms 1. general considerations. *IMA Journal of Applied Mathematics*, 6(1):76–90.

Delille, B., Harlay, J., Zondervan, I., Jacquet, S., Chou, L., Wollast, R., Bellerby, R. G., Frankignoulle, M., Borges, A. V., Riebesell, U., et al. (2005). Response of primary production and calcification to changes of pCO_2 during experimental blooms of the coccolithophorid *Emiliania huxleyi*. *Global Biogeochemical Cycles*, 19(2).

Eggers, S. L., Lewandowska, A. M., Barcelos e Ramos, J., Blanco-Ameijeiras, S., Gallo, F., and Matthiessen, B. (2014). Community composition has greater impact on the functioning of marine phytoplankton communities than ocean acidification. *Global Change Biology*, 20(3):713–723.

Engel, A., Cisternas Novoa, C., Wurst, M., Endres, S., Tang, T., Schartau, M., and Lee, C. (2014). No detectable effect of CO_2 on elemental stoichiometry of *emiliania huxleyi* in nutrient-limited, acclimated continuous cultures. *Marine Ecology Progress Series*, 507:15–30.

Engel, A., Thoms, S., Riebesell, U., Rochelle-Newall, E., and Zondervan, I. (2004). Polysaccharide aggregation as a potential sink of marine dissolved organic carbon. *Nature*, 428(6986):929–932.

Engel, A., Zondervan, I., Aerts, K., Beaufort, L., Benthien, A., Chou, L., Delille, B., Gattuso, J.-P., Harlay, J., Heemann, C., et al. (2005). Testing the direct effect of CO_2 concentration on a bloom of the coccolithophorid *Emiliania huxleyi* in mesocosm experiments. *Limnology and Oceanography*, 50(2):493–507.

Fasham, M., Ducklow, H., and McKelvie, S. (1990). A nitrogen-based model of plankton dynamics in the oceanic mixed layer. *Journal of Marine Research*, 48(3):591–639.

Feely, R. A., Sabine, C. L., Lee, K., Berelson, W., Kleypas, J., Fabry, V. J., and Millero, F. J. (2004). Impact of anthropogenic CO_2 on the $CaCO_3$ system in the oceans. *Science*, 305(5682):362–366.

Fernández-Castro, B., Pahlow, M., Mouriño-Carballido, B., Marañón, E., and Oschlies, A. (2016). Optimality-based *Trichodesmium* diazotrophy in the North Atlantic subtropical gyre. *Journal of Plankton Research*.

Findlay, H. S., Calosi, P., and Crawfurd, K. (2011). Determinants of the PIC: POC response in the coccolithophore *Emiliania huxleyi* under future ocean acidification scenarios. *Limnology and Oceanography*, 56(3):1168–1178.

Fletcher, R. (1970). A new approach to variable metric algorithms. *The Computer Journal*, 13(3):317–322.

Geider, R., Osborne, B., and Raven, J. (1985). Light dependence of growth and photosynthesis in *Phaeodactylum tricornutum* (*Bacillariophyceae*). *Journal Phycology*, 21(609-6):19.

Gibson, G. and Spitz, Y. (2011). Impacts of biological parameterization, initial conditions, and environmental forcing on parameter sensitivity and uncertainty in a marine ecosystem model for the Bering sea. *Journal of Marine Systems*, 88(2):214–231.

Goldfarb, D. (1970). A family of variable-metric methods derived by variational means. *Mathematics of Computation*, 24(109):23–26.

Haario, H., Saksman, E., and Tamminen, J. (2001). An adaptive metropolis algorithm. *Bernoulli*, pages 223–242.

Harding Jr, L. W., Fisher Jr, T. R., and Tyler, M. A. (1987). Adaptive responses of photosynthesis in phytoplankton: specificity to time-scale of change in light. *Biological Oceanography*, 4(4):403–437.

Harrison, W. and Platt, T. (1986). Photosynthesis-irradiance relationships in polar and temperate phytoplankton populations. *Polar Biology*, 5(3):153–164.

Iglesias-Rodriguez, M. D., Halloran, P. R., Rickaby, R. E., Hall, I. R., Colmenero-Hidalgo, E., Gittins, J. R., Green, D. R., Tyrrell, T., Gibbs, S. J., von Dassow, P., et al. (2008). Phytoplankton calcification in a high-CO_2 world. *Science*, 320(5874):336–340.

Joassin, P., Delille, B., Soetaert, K., Harlay, J., Borges, A. V., Chou, L., Riebesell, U., Suykens, K., and Grégoire, M. (2011). Carbon and nitrogen flows during a bloom of the coccolithophore *Emiliania huxleyi*: Modelling a mesocosm experiment. *Journal of Marine Systems*, 85(3):71–85.

Kidston, M., Matear, R., and Baird, M. E. (2011). Parameter optimisation of a marine ecosystem model at two contrasting stations in the sub-antarctic zone. *Deep Sea Research Part II: Topical Studies in Oceanography*, 58(21):2301–2315.

Kreus, M. and Schartau, M. (2015). Variations in the elemental ratio of organic matter in the central baltic sea: Part I–sensitivities of annual mass flux estimates to model parameter variations. *Continental Shelf Research*, 100:46–63.

Langer, G., Nehrke, G., Probert, I., Ly, J., and Ziveri, P. (2009). Strain-specific responses of *emiliania huxleyi* to changing seawater carbonate chemistry. *Biogeosciences*, 6(11):2637–2646.

Lewislg, M. R. and Smith, J. C. (1983). A small volume, short-incubation-time method for measure-ment of photosynthesis as a function of incident irradiance. *Marine Ecology Progress Series*, 13:99–102.

Marra, J. and Heinemann, K. (1982). Photosynthesis response by phytoplankton to sunlight variability. *Limnology and Oceanography*, 27(6):1141–1153.

Matear, R. J. (1995). Parameter optimization and analysis of ecosystem models using simulated annealing: a case study at station p. *Journal of Marine Research*, 53(4):571–607.

Metropolis, N., Rosenbluth, A. W., Rosenbluth, M. N., Teller, A. H., and Teller, E. (1953). Equation of state calculations by fast computing machines. *The Journal of Chemical Physics*, 21(6):1087–1092.

Orr, J. C. (1999). Ocean Carbon-Cycle Model Intercomparison Project (OCMIP): Phase I (1995-1997). *IGBP/GAIM Report Series*, 7.

Orr, J. C., Fabry, V. J., Aumont, O., Bopp, L., Doney, S. C., Feely, R. A., Gnanadesikan, A., Gruber, N., Ishida, A., Joos, F., et al. (2005). Anthropogenic ocean acidification over the twenty-first century and its impact on calcifying organisms. *Nature*, 437(7059):681–686.

Pahlow, M., Dietze, H., and Oschlies, A. (2013). Optimality-based model of phytoplankton growth and diazotrophy. *Marine Ecology Progress Series*, 489:1–16.

Pahlow, M. and Oschlies, A. (2009). Chain model of phytoplankton P, N and light colimitation. *Marine Ecology Progress Series*, 376:1–16.

Pahlow, M., Vézina, A. F., Casault, B., Maass, H., Malloch, L., Wright, D. G., and Lu, Y. (2008). Adaptive model of plankton dynamics for the north atlantic. *Progress in Oceanography*, 76(2):151–191.

Platt, T., Denman, K., and Jossby, A. (1977). Modelling the productivity of phytoplankton. *The Sea*, 6:807–856.

Riebesell, U., Bellerby, R., Grossart, H.-P., and Thingstad, F. (2008). Mesocosm CO_2 perturbation studies: from organism to community level. *Biogeosciences (BG)*, 5(4):1157–1164.

Ruiz, J., Prieto, L., and Ortegón, F. (2002). Diatom aggregate formation and fluxes: a modeling analysis under different size-resolution schemes and with empirically determined aggregation kernels. *Deep Sea Research Part I: Oceanographic Research Papers*, 49(3):495–

515.

Schartau, M., Engel, A., Schröter, J., Thoms, S., Völker, C., and Wolf-Gladrow, D. (2007). Modelling carbon overconsumption and the formation of extracellular particulate organic carbon. *Biogeosciences*, 4(4):433–454.

Schartau, M., Wallhead, P., Hemmings, J., Löptien, U., Kriest, I., Krishna, S., Ward, B. A., Slawig, T., and Oschlies, A. (2016). Reviews and syntheses: Parameter identification in marine planktonic ecosystem modelling. *Biogeosciences Discussions*, pages 1–79.

Shanno, D. F. (1970). Conditioning of quasi-Newton methods for function minimization. *Mathematics of Computation*, 24(111):647–656.

Sibly, R. M., Brown, J. H., and Kodric-Brown, A. (2012). *Metabolic ecology: a scaling approach*. John Wiley & Sons.

Skartveit, A., Cleveland, F., and de Lange, T. (2001). Radiation Yearbook no. 37, Meteorological Report Series, University of Bergen. Technical report, University of Bergen Geophysical Institute, Bergen, Norway.

Smith, S. L., Pahlow, M., Merico, A., and Wirtz, K. W. (2011). Optimality-based modeling of planktonic organisms. *Limnology and Oceanography*, 56(6):2080–2094.

Soetaert, K. and Petzoldt, T. (2010). Inverse modelling, sensitivity and monte carlo analysis in r using package fme. *Journal of Statistical Software*, 33.

Verdugo, P., Alldredge, A. L., Azam, F., Kirchman, D. L., Passow, U., and Santschi, P. H. (2004). The oceanic gel phase: a bridge in the DOM–POM continuum. *Marine Chemistry*, 92(1):67–85.

Wolf-Gladrow, D. A., Zeebe, R. E., Klaas, C., Körtzinger, A., and Dickson, A. G. (2007). Total alkalinity: The explicit conservative expression and its application to biogeochemical processes. *Marine Chemistry*, 106(1):287–300.

Zondervan, I., Rost, B., and Riebesell, U. (2002). Effect of CO_2 concentration on the PIC/POC ratio in the coccolithophore *Emiliania huxleyi* grown under light-limiting conditions and different daylengths. *Journal of Experimental Marine Biology and Ecology*, 272(1):55–70.